

NOVEL COATING METHODS ON CENTRIFUGALLY-SPUN POLYMER FIBERS FOR
APPLICATIONS IN LITHIUM-ION BATTERIES

A Thesis

by

JONATHAN G. AYALA

Submitted to the Graduate College of
The University of Texas Rio Grande Valley
In partial fulfillment of the requirements for the degree of

MASTER OF SCIENCE IN ENGINEERING

May 2021

Major Subject: Mechanical Engineering

NOVEL COATING METHODS ON CENTRIFUGALLY SPUN POLYMER FIBERS FOR
APPLICATIONS IN LITHIUM-ION BATTERIES

A Thesis
by
JONATHAN G. AYALA

COMMITTEE MEMBERS

Dr. Mataz Alcoutlabi
Chair of Committee

Dr. Horacio Vasquez
Committee Member

Dr. Javier Ortega
Committee Member

May 2021

Copyright 2021 Jonathan Ayala

All Rights Reserved

ABSTRACT

Ayala, Jonathan, Novel Coating Methods on Centrifugally Spun Polymer Fibers for Applications in Lithium-ion Batteries. Master of Science Engineering (MSE), May 2021 58 pp, 3 tables, 32 figures, 65 references, 16 titles

The work presented in this thesis focuses on the processing, characterization, and electrochemical results of centrifugally spun composite carbon fiber electrodes for application as anode material in lithium-ion batteries. The work is presented as a compilation of two major projects. First, the use of novel Co_3O_4 wet coatings to increase the capacity of carbon fibers produced from Polyacrylonitrile (PAN). In this work, PAN fibers are produced via the Forcespinning method, and were heat treated by oxidation in air at $200\text{ }^\circ\text{C}$ for four hours, and subsequent carbonization at $600\text{ }^\circ\text{C}$ for six hours. The electrochemical performance of the $\text{Co}_3\text{O}_4/\text{C}$ composite-fiber anode with different active material loading was evaluated by using galvanostatic charge/discharge, rate performance, cyclic voltammetry, and electrochemical impedance spectroscopy experiments. The CCF anode delivered a specific charge capacity of 632 and 420 mAh g^{-1} after 100 cycles at 100 and 200 mA g^{-1} , respectively, and exhibited good rate capability.

This work is then followed by the electrochemical performance of silicon nanoparticles imbedded in fiber composites derived from polyvinylpyrrolidone (PVP), and their enhanced cyclability when using Sodium Carboxymethyl Cellulose (Na-CMC) polymer coating. The composite anodes were fabricated via a similar sol-gel synthesis method, however, annealing of

Si/PVP fibers was done at low temperature (160 °C), and carbonization was carried out under inert gas to prevent further oxidation of the silicon nanoparticles in the PVP fibers. The silicon/ carbon fiber composites, together with Na-CMC delivered a specific capacity of 2300 mAhg⁻¹ for the first 20 cycles and showed an initial columbic efficiency of 83% when tested in a standard lithium electrolyte with FEC as additive. The positive effect of Na-CMC coating on the carbon fiber/ silicon composite was seen in the diminished loss of capacity in the first cycle by up to 20%. These results suggest that Na-CMC/ CMC structures can enhance the cyclability and stable SEI formation of centrifugally spun carbon fiber composites.

DEDICATION

The completion of my master's degree would not have been possible without the love and support of my family. Thank you to my father Efren Ayala, and my mother Antonia Silva, who brought me to this country in order to give me the opportunity of a better future. Thank you for instilling in me the importance of faith and for showing me how life goes on in spite of challenges we face. This degree is for my late Grandfather Jesus and Grandmother Concepcion who would have been proud of their grandson you raised. "Los Amo muchisimo".

To my soon to be wife, for her love and affection, and for her reassuring words which were always there when I needed them. Thank you for being my rock, for helping me become a better person. I love you and will never be able to thank you enough for the patience and support you show.

To my siblings, Efren, David, Daniela and Emily, thank you for always giving me a reason to laugh and love, and to show you we are capable of accomplishing great things.

ACKNOWLEDGEMENTS

A special thanks to Dr. Mataz Alcoutlabi, chair of my thesis committee for all of his mentoring, and his constant push to instill hard work and dedication. Many thanks to my thesis committee members, Dr. Javier Ortega, and Dr. Horacio Vasquez, as well as Dr. Padilla for all their help along the years.

I would also like to thank my research group, thank you guys for keeping a light-hearted spirit, and making the lab feel like a family. Thank you for the many inquisitive arguments that led to us becoming better every day. I hope that we can stay lifelong friends.

TABLE OF CONTENTS

	Page
ABSTRACT.....	iii
DEDICATION.....	v
ACKNOWLEDGEMENTS.....	vi
TABLE OF CONTENTS.....	vii
LIST OF TABLES.....	ix
LIST OF FIGURES.....	x
CHAPTER I: INTRODUCTION.....	1
CHAPTER II: LITERATURE REVIEW.....	3
2.1 Lithium-ion Batteries.....	3
2.2 Working Principle of LIBs.....	4
2.2 Cathode Materials.....	4
2.3 Anode Materials in LIBs.....	6
2.4 Carbonaceous Anode Electrodes, Carbon Fiber Anodes.....	8
2.6 Binder Materials.....	10
2.5 Anode/Electrolyte Interface.....	11
CHAPTER III: STATE OF THE ART INSTRUMENTATION.....	13
3.1 Material Processing Equipment.....	13
3.1.1 Forc spinning Cyclone.....	13
3.1.2 Heat Treatment Furnaces.....	14
3.2.1 Zeiss Scanning Electron Microscope.....	15
3.2.2 Xray Photoelectron Spectroscopy.....	15
3.3 Electrochemical Testing Hardware and Software.....	15
CHAPTER IV: EXPERIMENTAL PROCEDURE.....	18
3.1 Fabrication of Carbon Fibers from PAN.....	18
3.2 Preparation of Co ₃ O ₄ -Coated Carbon Fibers.....	18

3.3 Fabrication of Carbon Fibers from PVP	19
3.4 Fabrication of Silicon/Carbon Fiber Composite Anodes	20
3.5 Fabrication of Silicon Slurry Anodes.....	20
3.6 Electrochemical Evaluation Tests	22
CHAPTER V: RESULTS AND DISCUSSION.....	23
4.1 Morphology and Characterization.....	23
4.1.1 Carbon Fibers (CFs) & Composite Co ₃ O ₄ /C Fibers (CCFs)	23
4.1.3 Silicon/Carbon Fiber Composite Anodes.....	27
4.1.3 CMC Coated Silicon/Carbon Fiber Composite Anodes	28
4.1.4 Silicon Slurry Anodes	31
4.2 Electrochemical Results	35
4.2.1 Carbon Fibers & Co ₃ O ₄ /Carbon Fiber Composite Anodes.....	35
4.2.2 Silicon/Carbon Fiber Composite Anodes.....	40
4.2.3 Silicon Slurry Anodes	41
CHAPTER VI: CONCLUSION	47
CHAPTER VII: FUTURE WORK.....	49
REFERENCES	50
APPENDIX.....	55
BIOGRAPHICAL SKETCH	58

LIST OF TABLES

Table 1: Components of processed silicon slurry anodes.....	22
Table 2: Electrochemical Impedance Spectra Modeling values.....	37
Table 3: State of the Art Instrumentation.....	50

LIST OF FIGURES

Figure 1 . Lithium ion Battery Model [5]	3
Figure 2. Anode Materials in LIBs [13].....	6
Figure 3. SEM images of carbon nanofibers.....	9
Figure 4. Forcespinning Cyclone	13
Figure 5. Heat Treatment Equipment used for polymer fiber processing.....	14
Figure 6. A. Scanning electron microscope (SEM) coupled with energy-dispersive X-ray spectroscopy (EDS), B. X-Ray photoelectron spectroscopy (XPS)	14
Figure 7. MBRAUN (LABstar pro).....	15
Figure 8. A. LANHE battery testing system (CT2001A). B. Arbin automatic battery cycler C. Biologic (MCS810). D. Metrohm Autolab	16
Figure 9. Schematic showing processing of composite fiber electrodes	19
Figure 10. A. SEM and size distribution of CF anode electrodes at 10,000X. B. 5,000, Co ₃ O ₄ /C. C. Composite Fibers at 10,000X, D. 5,000 X. E. a higher concentration Co ₃ O ₄ /C Composite Fibers at 2000X, and F. 5,000 X magnifications. Inserts show the fiber diameter distribution (histograms).	24
Figure 11. HRTEM image of Co ₃ O ₄ nanoparticles embedded in carbon fibers. B. Carbon, C. Cobalt D. Oxygen, E. Nitrogen of the Co ₃ O ₄ /C composite fibers.....	24
Figure 12. TGA curves of CF, CCF30, CCF50, and CCF70 samples, obtained at 10 °C min ⁻¹	26
Figure 13. A. SEM images of fiber anodes from carbonized Si/PVP fibers. B. In-lens image at high magnification of carbonized Si/PVP fibers. C. SEM image used to probe EDS maps. D. EDS maps of fiber anodes from carbonized Si/PVP fibers.	27

Figure 14 A. SEM images of fiber anodes from carbonized Si/PVP fibers coated with CMC. B. In-lens image at high magnification of carbonized Si/PVP fibers coated with CMC. C. SEM image at high magnifications. D. In-lens SEM image at high magnification.	28
Figure 15 EDS Mapping of silicon carbon fiber anodes coated with NaCMC, sputter coated with Gold.	29
Figure 16 XPS C1s scans of A. PVP/Si and B. PVP/Si/CMC and Si2P scans of A. PVP/Si and B. PVP/Si/CMC	30
Figure 17 A. SEM image of silicon slurry anodes. B. EDAX Mapping of silicon composition.....	31
Figure 18 A. SEM image of silicon/carbon fiber slurry anodes. B. SEM image of silicon/carbon fiber anodes at high magnification.	31
Figure 19: EDS Mapping of silicon slurry anodes with carbon fiber as conductive additive.....	32
Figure 20 SEM image of silicon/porous carbon fiber slurry anodes derived from PAN/PMMA fibers after carbonization.	32
Figure 21 SEM images of Co ₃ O ₄ short fibers imbedded in silicon slurry anodes.....	33
Figure 22 EDS Mapping showing Co ₃ O ₄ short fibers imbedded in silicon slurry anodes B Elemental Overlay C. Cobalt Map D. Silicon Map	34
Figure 23 A. Cyclic voltammetry of CF and CFF50 B. in a half-cell configuration and cycled between 0 and 3.0 V at a scan rate of 0.2 mV s ⁻¹	35
Figure 24 Galvanostatic charge/discharge profiles of A. CF, B. CCF50 at 100 mA g ⁻¹ , and C. CCF30(C), D. CCF70(D) at 200 mA g ⁻¹ at a cut-off voltage between 0.1 and 3V.	36
Figure 25 A. Cycle performance of CFs and CCFs at a charge/discharge rate of 200 mA g ⁻¹ B. Rate performance of CF, CCF30, and CCF70 in Li-ion half cells.....	38
Figure 26 A. Electrochemical impedance results (Nyquist plots) of fresh and aged Li-ion half cells containing CCF electrodes with different Co ₃ O ₄ constrictions. B. Impedance table showing R _s , R _P , and equivalent circuit model of the CCF anodes.	39

Figure 27. Cyclic Voltammetry of A. PVP/Si Electrode B. PVP/Si/CMC Electrode, and C. PVP/Si/CMC Electrode with 10% FEC additive in the electrolyte	41
Figure 28 Cyclic Voltammetry of A. PVP/Si Electrode B. PVP/Si/CMC Electrode, and C. PVP/Si/CMC Electrode with 10% FEC additive in the electrolyte	42
Figure 29 Charge Capacity (mAh/g) for 10 cycles for Silicon/ PVP Fiber electrodes	42
Figure 30 Electrochemical Impedance Spectroscopy of Silicon/ PVP Fiber electrodes	43
Figure 31. A. Cyclic Voltammetry of silicon slurry anodes. B. Cyclic Voltammetry of silicon/ carbon fiber slurry anodes. C. Charge Discharge profiles of silicon slurry anodes. D. Charge Discharge profiles of silicon/carbon fiber slurry anodes.....	45
Figure 32. A. Cycle Performance of silicon slurry anodes. B. Cycle Performance of silicon/ carbon fiber slurry anodes. C. Impedance plots of silicon and silicon/carbon fiber slurry anodes.....	46

CHAPTER I

INTRODUCTION

The ability to store energy has driven innovation throughout history. In Electrochemistry it occurred first through the invention of electric batteries in the 1800s [1]. The earliest battery, Alessandro Volta's electrical pile, consisted of stacked copper and zinc plates, separated by a form of brine-soaked paper disks. Although Volta did not fully understand the implications nor the fundamental driving force of his battery, this "voltaic pile" incited many debates and eventually led to the formulation of the electrochemical theory [2].

In the early part of the 20th century, a new understanding of the redox reactions taking place inside batteries allowed for the invention of various combinations of materials and cell designs. Consequently, Potassium hydroxide (Alkaline) electrolyte combined with zinc and manganese dioxide electrodes became the most common type of battery technology used by the latter half of the 20th century. [3]

The concept of using reversible redox reactions led to the introduction of rechargeable (secondary) batteries with electrodes such as lead acid and manganese dioxide-zinc paired with electrolytes such as H₂SO₄. However, revolutionary advances in secondary batteries arrived with the production of Lithium Ion Batteries (LIBs) roughly 30 years ago when Sony and Asahi Kasei Corporations commercialized the first LIBs. [4] Since their development, the ability to design

products for portability and high energy density has enabled the acceleration of convenient and efficient consumer electronics. Nevertheless, continued development of positive and negative electrode chemistries will play an important role in unlocking increased power storage potential.

The present work is a culmination of two years investigating the performance and behavior of different anode materials. It provides a focus on the synthesis, morphological characterization, and electrochemical performance of nanostructured electrodes including carbon-fiber based composites of cobalt and silicon, as well as the incorporation of some composite fibers into silicon slurry electrodes as anodes for LIBs. Their synthesis is derived from centrifugally force-spun polymers, with processing of some fibrous polymers prior and post heat treatment. Novel coating methods for carbon composite fibers are explored as alternative methods of producing composite carbon fiber anodes for LIBs.

CHAPTER II

LITERATURE REVIEW

2.1 Lithium-ion Batteries

A Lithium-ion Battery is a system with five main components. Cathode, Anode, Electrolyte, Separator, and two current collectors.

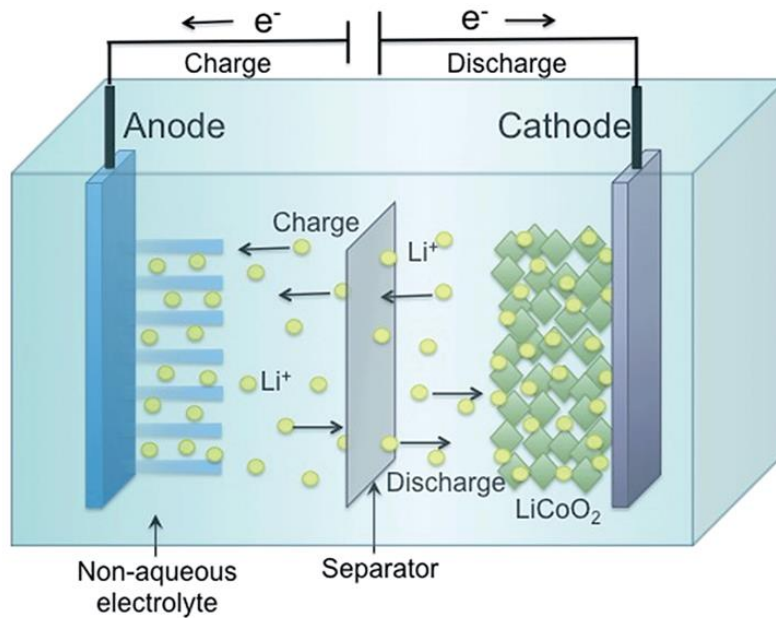


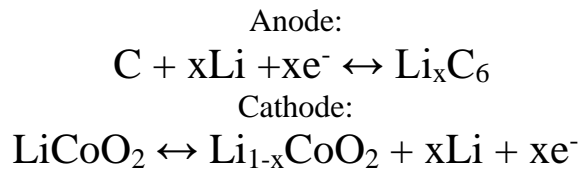
Figure 1 . Lithium ion Battery Model [5]

All these components play an important role in the functionality of a LIB. Cathode materials provide lithium to the cell and dictate the working voltage of a battery [6]. Lithium metal oxides (LMOs) are used to provide lithium in a LIB due to their layered nature which provides lithium ions a gap to become inserted/reinserted. The anode, or negative electrode, provides lithium

storage when the cell is charged, and is also stored between layers of graphite anodes. The medium through which the ion flows from one extreme to the other is the electrolyte, and is typically composed of an ionic salt, while the separator, which prevents the anode and cathode from contact, is usually made of porous materials such as microfiber glass. Current collectors (aluminum for cathodes and copper for anode) are used to ensure proper connection between electrodes and the external circuits

2.2 Working Principle of LIBs

At a certain voltage upon charging, the cathode begins to oxidize and will lose lithium ions. The ionically conductive electrolyte allows these ions to travel across the cell making their way into the structure of the anode where chemical potential energy in the form of charged products $\text{Li}_{1-x}\text{CoO}_2$ and Li_xC_6 is converted to electrical energy at lower voltages [7]. Upon discharge or closing of the external circuit, chemical potential energy stored in the anode will return to its original lower energy state by losing lithium ions which travel back and intercalate into the cathode, and electrons, which flow through the copper current collector back to the cathode through the external circuit. The following equation shows the chemical reaction that happens in a typical LiCoO_2 cathode and a graphite anode cells.



2.2 Cathode Materials

LIB components are dependent on the cathode material to supply lithium. For this reason, the cathode electrode is a very important primary component. For years, the preferred structure

of cathodic compounds has been layered or spinel, in order to facilitate lithium intercalation into the crystal structure of the material. Metals that form layered ionic crystal structures which can allow for the intercalation of lithium ions include cobalt, nickel, iron, and manganese. The prominence of cobalt in cathode materials is due to its ability to add strength and energy density to the cathode crystal structure. However, its affinity to nearby atoms decreases energy density by preventing the lithium ion from deintercalation. Another metal, nickel, can increase energy density by allowing more lithium ions to be deintercalated. However, nickel does not provide proper structural support, and in some cases, the loosely bounded nickel can fall in between the cathode layers, taking up space and restricting the flow of lithium ions [8]. Most cathode chemistries used today have coupled both of these materials in order to optimize cathode performance. Moreover, the development of ternary nickel-rich cathodes chemistries such as nickel-cobalt-aluminum, and quaternary cathodes such as nickel-cobalt-manganese-aluminum, have introduced ways to increase energy density and efficiency, while allowing for the reduction of cobalt content, associated with high costs and humanitarian questionability due to child labor.

Much importance is placed on the electrolyte of a cell. Organic solvent based liquid electrolytes have dominated the industry for years, typically mixed to dilute an ionic salt (usually LiPF_6 or $\text{LiN}(\text{CF}_3\text{SO}_2)_2$) to form an ionically conductive medium. Early cells used Propylene carbonate (PC) and diethyl carbonate (DEC); ethylene carbonate and γ -butyrolactone (γ -BL), methyl ethyl carbonate (MEC), methyl propionate (MP) and dimethyl carbonate (DMC). However, Organic solvent's flammable properties have been problematic in the past. Especially at high voltages, vapor pressures and dendrite formation can be dangerous as they may lead to short circuits and even fires or explosions. Recent advances in electrolyte additives such as fluoroethylene carbonate (FEC), have gained attention due to their high resistance to

flammability. However, research into solid electrolytes including polymer and gel electrolytes, are among the most promising alternatives being researched. [9-12]

2.3 Anode Materials in LIBs

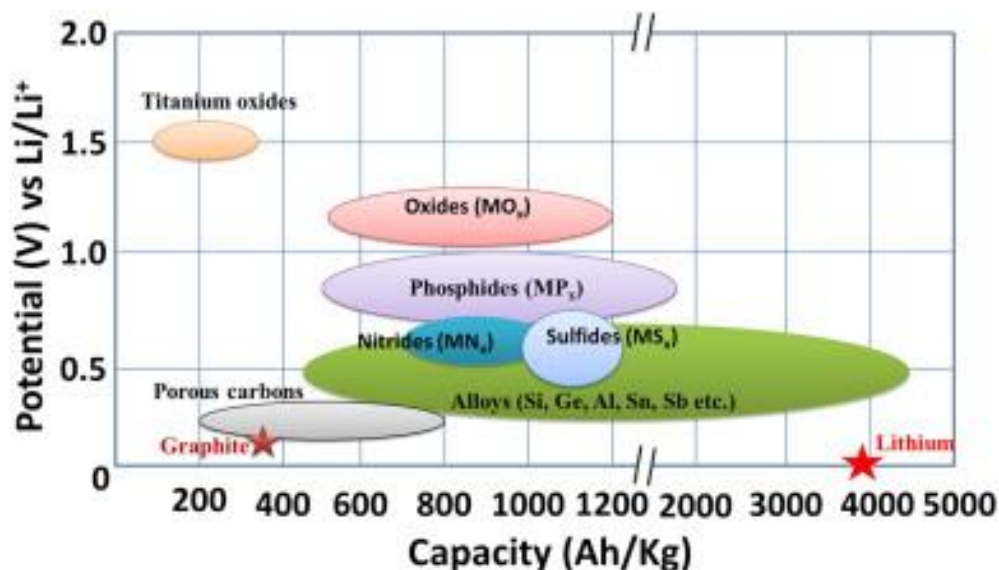


Figure 2. Anode Materials in LIBs [13]

The anode in a LIB can be considered just as important as the cathode since it allows for the reversible storing of lithium ions. Graphite is currently the most widely used material in LIB anodes due to its long cycle life, low manufacturing cost, and low intercalation voltage[6, 13, 14]. Its theoretical capacity of 372 mAhg^{-1} , is low compared to other materials. However, given that cathodes are the limiting factor in a LIB and do not surpass 300 mAhg^{-1} , increasing the capacity of the anode does not necessarily result in an increase of energy density when paired with a low capacity cathode. Thus, graphite has and will likely continue to be an important anode material for years to come. Nevertheless, development of future generations of cathodes, will likely require anodes with increased specific capacity. For this reason, current LIB anode research is focused on implementing novel material chemistries, designing nano/micro structured

electrodes, and identifying electrolyte additive/binder interactions to increase efficiency and specific capacity of anode electrodes. Figure 2 provides different materials with potential for their use as anodes in LIBs, and their respective theoretical capacities as well as working voltages vs Li/Li⁺.

Anode materials react to lithium ions via three main mechanisms: intercalation, conversion, or alloying. The intake of lithium ions into the crystal structure can occur as orderly intercalation into layered structures i.e., TiO₂, Li₄Ti₄O₁₂, MoS₂, SnO₂. An advantage to a layered structure is parallel charge paths, leading to favorable micro kinetic properties. In the case of graphite anodes, lithium ions are accommodated between the graphite layers, and results in ordered reversibility, leading to cycle stability and a resulting in a long-lasting electrode. TiO₂ has also been investigated due to the reversibility of the spinel Li₄Ti₅O₁₂ structure does not vary much upon lithiation [15, 16]. These anodes show good cycle life, low manufacturing cost, and high-power capability.

Conversion reactions are electrochemical reactions of binary transition metal compounds metal (oxides, sulfides, nitrides, and phosphides) with lithium. These compounds can increase the theoretical capacity of the electrode, however, they have been associated with high voltages, and lower capacity retention [17]. Transition metal oxides are among the most investigated conversion materials due to their high reactivity to lithium. [18] Among these, cobalt oxide electrodes have been considered among top candidates due to their high theoretical capacity (890mAhg⁻¹) for Co₃O₄. However, loss of contact to conductive additive, volume change upon cycling, and the continual decomposition of the electrolyte provide challenging issues to overcome before they can be widely used as anode electrode materials. [18, 19]

Alloying anodes have also been known to increase specific capacity of anode electrodes, these alloying elements include Si, Sn, Al, Ge, Sb and others (shown in figure 2: green). An advantage to the alloying anodes is their low voltage and high theoretical capacity. However, similar to conversion materials, the increased uptake of multiple lithium ions per atom results in large volume variations in the crystal structure. Moreover, this high capacity leads to large internal stresses in the anode, which results in prevention of a stable formation of the solid electrolyte interface (SEI) layer and eventually leads to pulverization of the anode after prolonged cycling [20]. Nevertheless, alloying materials, specifically silicon, hold promising futures as anode electrodes in LIBs, and are well under research [21-30]. Most of these include silicon in the low content range of 20-30% of the total weight of the anode electrode in order to relieve some of the stress provided by the lithiation/de-lithiation cycles of silicon.

2.4 Carbonaceous Anode Electrodes, Carbon Fiber Anodes

In the field of electrochemistry, carbonaceous structures including carbon nanotubes, carbon nanowires, and porous carbon have been researched as anode materials due to their high conductivity, low voltage, and stable reversible capacity of 372 mAhg^{-1} . Carbon coatings of nanoparticles by CVD or sol gel methods, hollow carbonaceous structures, nanotubes, and other carbon composites are generally thought to restrict volume expansion and allow a stable cycling of LIBs. [31]

More recently, techniques such as Electrospinning and centrifugal-force spinning have been employed to mass produce carbon fibers (CFs) and CF composite anodes [32-34]. These “binder-free” anode is usually in the form of flexible, conductive structure, with domains

belonging to amorphous or semi crystalline phases within the carbon fibers. One of the main drawbacks of electrospinning is high voltages required to generate fibers. While centrifugal spinning procedure prevents the need for this, high concentration of metal oxide precursor increases the viscosity and eventually leads to phase separation in the solution, yielding insufficient generation of fibers via centrifugal spinning method. Moreover, some materials yield fibers with large agglomerations of particles which is unwanted for higher capacity.[35].

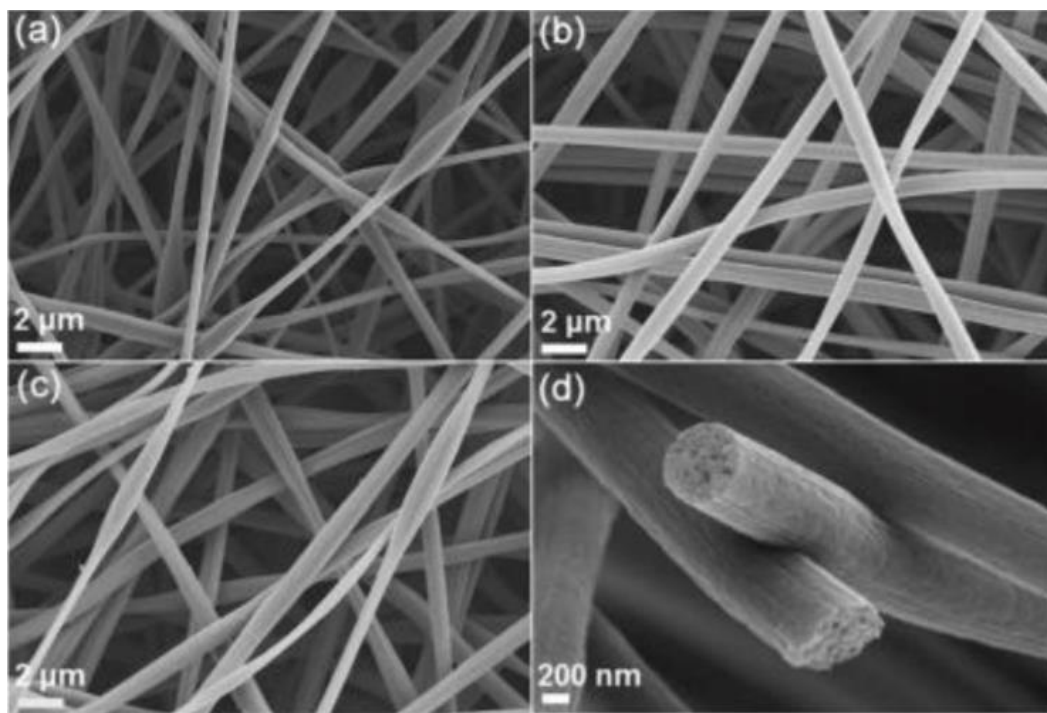


Figure 3. SEM images of carbon nanofibers

Perhaps the most attractive feature of carbon fibers is the high surface area to volume ratio, which provides more active sites for the lithium ions to intercalate, thereby increasing its initial capacity. However, high aspect ratio also contributes to the formation of a large SEI layer when compared to slurry anodes with less surface area. Polyacrylonitrile (PAN) has been widely used as a precursor to obtain carbon fibers from the electrospinning and centrifugal spinning due

to its high yield of up to 80% [36]. However, the use of harmful solvents such as Dimethylformamide (DMF) has accelerated the use for polymers such as Polyvinyl Pyrrolidone (PVP) among other polymers which can be dissolved in water and/or ethanol and produce carbon fibers upon heat treatment [37, 38].

Metal oxide/carbon fiber anodes have been investigated in the past [39-41], the main objective being encapsulating metal oxide particles inside the fiber, thus restricting the particle's volume expansion and allowing for increased cycle stability. These carbon fiber composites are typically prepared by dissolving a metal-oxide precursor in the polymer solution and utilizing an oxidative temperature in the heat treatment to yield metal-oxide nanoparticles within the carbon fibers. While cyclability of the anode is improved by encapsulating active materials with carbon fibers, specific capacity can also be affected if the carbon fiber is thick by restricting access to lithium to these high capacity nanoparticles. In cases where the carbon fibers are ideally located within the fibers, increased performance has been reported when compared to carbon fibers alone. However, after repeated cycles, this stress within the fibers can lead to decreased electrochemical performance due to crack propagation and pulverization of the fiber anode. [40, 42]

2.6 Binder Materials

In electrochemistry, few generalizations can be made in terms of material performance. For example, there is no one binder or electrolyte additive able to enhance the performance of all anode electrodes. Instead, research in choice of binder material and electrolyte additives are segmented into studies of specific material interactions. For years, the preferred binder for graphite anodes and commercial cathodes has been Polyvinylidene fluoride (PVDF), although the use of PAN and other polymers has also been explored [43]. However, the effort of

incorporating high capacity active materials has often been thought to require different binders with high elastic properties to allow for volume expansion of the anode electrode. However, more recently the interaction or binding mechanism of the active material to the binding polymer has been given more importance [27, 44].

For silicon anodes, the importance of Covalent bonding of the polymer to silicon in LIB anodes has mostly been highlighted through Polyacrylic Acid (PAA) and sodium Carboxymethylcellulose (CMC) [44]. CMC is an environmentally friendly polysaccharide abundant in most plants, composed of hydroxyl and carboxyl groups attached to a carbonaceous backbone. Similar to silicon, CMC is an attractive binder alternative due to its abundance in nature. Acidic groups in this polymer have significantly enhanced the electrochemical performance of silicon anodes. Although considered a stiff polymer with low elongation at break, CMC has been successful in silicon based anodes due to the covalent bonding of the carboxylic acid groups to the surface of the native oxide layer in silicon nanoparticles [26, 27, 45]. Studies with CMC have also shown that CMC is stable in carbonate solvents as opposed to PVDF which is significantly swollen and becomes easily deformable. CMC therefore can aid in stabilizing the surface of silicon nanoparticles from further reacting with the electrolyte [46].

2.5 Anode/Electrolyte Interface

The electrolyte in a LIB is responsible for allowing lithium ions to travel from one electrode to the other. During the first charge process (lithium insertion into anode) formation of the solidification of some electrolyte results in the formation of the SEI layer. This nonionic by-product between the negative electrode (or positive) and the lithium electrolyte forms during the contributes to the initial irreversible capacity. Formation of the SEI is an unavoidable aspect of

LIB anodes, thus, apart from methods of prevention, methods of improving the interface of the anode/electrolyte has become an important goal in developing an efficient LIB. Techniques such as pre lithiation in which the anode is charged for one cycle prior to cell assemblage has been an effective method to decrease the irreversible capacity loss in the first cycle. Allowing for slow formation in the first cycle creates an SEI that protects the electrode from further reacting with the solvent, which can enhance the performance of the anode. However, pre lithiation has been criticized for its inefficiency in scaling or adoption into mass production of anodes [47]. Other methods to reduce the effects of this layer include passive SEI Formation (at lower charge rates), as well as electrolyte additives such as vinyl carbonate, fluoroethylene carbonate, butanedinitrile, chloroethylene carbonate, and others which have been used due to their film forming ability in electrolytes, which can be used to further stabilize the reaction mechanisms that underlie the formation of the SEI [9, 11, 48, 49].

In this thesis, we investigate the performance of novel coatings on nanofibers, to produce composite carbon fibers for applications in LIBs. The development of efficient ways of increasing active material concentration is explored first through the wet coating of Co_3O_4 on PAN fibers derived from centrifugally spun method. This work is then followed by the development of CMC coatings on Silicon/PVP fibers produced via centrifugal spinning, and their effect on decreasing the impact of the SEI layer on the first cycle irreversible capacity loss. With the use of CMC, and FEC electrolyte additives, Novel coating methods explored in this work can enhance electrochemical performance and stabilize the reaction to electrolyte of the silicon carbon fiber anodes, while coatings of metal-oxides on pristine nanofibers showed an ability to form composite fibers with good dispersion and capacity retention for applications in LIBs. .

CHAPTER III

STATE OF THE ART INSTRUMENTATION

3.1 Material Processing Equipment

3.1.1 Forcespinning Cyclone

The process known as Forcespinning (FS) was developed by Lozano and Sarkar in 2009. At the time, it overcame the major setback with electrospinning, namely the requirement of high voltage and use of dangerous working current to slowly yield fibers (0.1gram/min). With a simpler design, FS uses centrifugal forces to overcome the surface tension of polymer jets in order generate fibers. This process allows for the higher yield in fiber generation of up to 1 gram per minute [50, 51]. In this thesis, the FS Cyclone (FiberRioL1000MD) was used to generate polymer composite fibers from PAN and PVP polymers.



Figure 4. Forcespinning Cyclone

3.1.2 Heat Treatment Furnaces

Further processing of polymer fibers required the use of an OTF-1200X tube furnace (MTI Corp. California, USA) for oxidative and carbonization heat treatments, as well as a Carbolite Gero (CWF 1300) for annealing of PVP and Si/PVP fibers.



Figure 5. Heat Treatment Equipment used for polymer fiber processing. **A.**OTF-1200X **B.** Carbolite GERO (CWF 1300)

3.1 Characterization Equipment

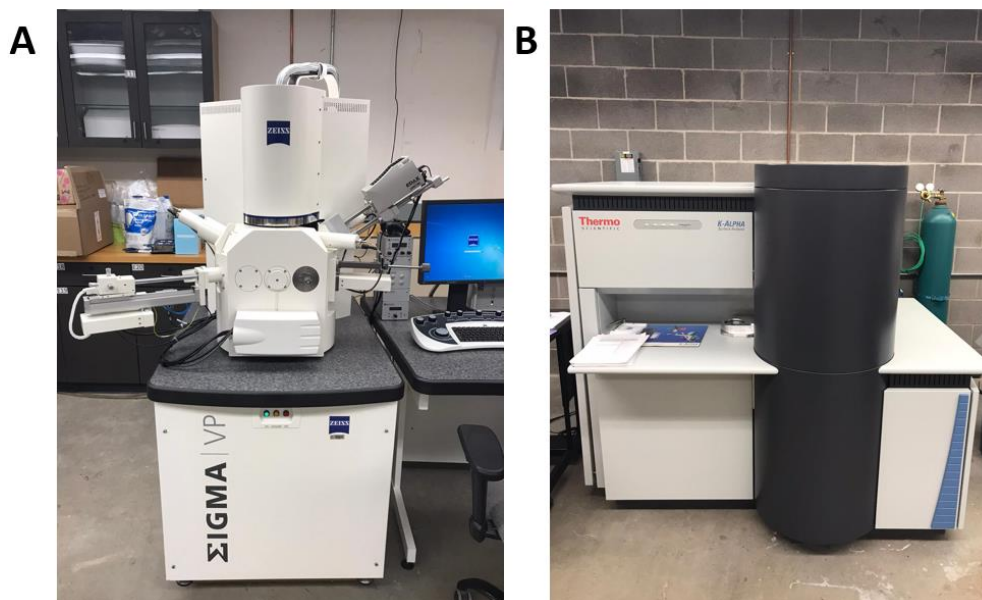


Figure 6. **A.** Scanning electron microscope (SEM) coupled with energy-dispersive X-ray spectroscopy (EDS), **B.** X-Ray photoelectron spectroscopy (XPS)

3.2.1 Zeiss Scanning Electron Microscope

Scanning electron microscopy (SEM) imaging and energy-dispersive X-ray spectroscopy (EDS) of polymer fibers, carbon fibers, and composite carbon fibers were collected using a Sigma VP Carl Zeiss scanning electron microscope with an attached EDAX detector (EDAX, Mahwah, NJ, USA).

3.2.2 X-ray Photoelectron Spectroscopy

X-Ray photoelectron spectroscopy (XPS) data were collected using a Thermo Scientific K-Alpha X-ray Photoelectron Spectrometer to characterize surface composition of the CFFs to evaluate binding environments present before and after heat treatment of Co₃O₄ coated PAN fibers.

3.3 Electrochemical Testing Hardware and Software

All lithium ion half cells were assembled using CR2032 coin cells by employing a lithium chip as the counter electrode inside a MBRAUN (LABstar pro) glove box filled with ultra-high purity argon with H₂O and O₂ concentrations of <0.5 ppm.

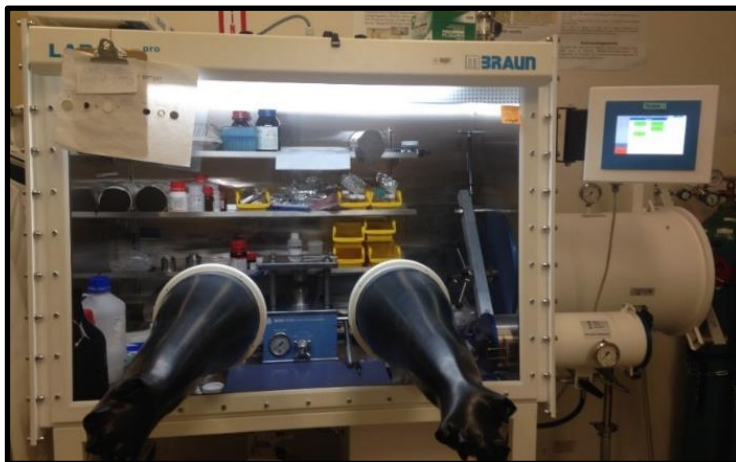


Figure 7. MBRAUN (LABstar pro)

Figure 7. MBRAUN (LABstar pro)

Cyclic voltammetry (CV) experiments were performed using Biologic (MCS810) at a scan rate of 0.2 mVs^{-1} over the range from 0.01 to 3.0 V (vs Li/Li⁺).

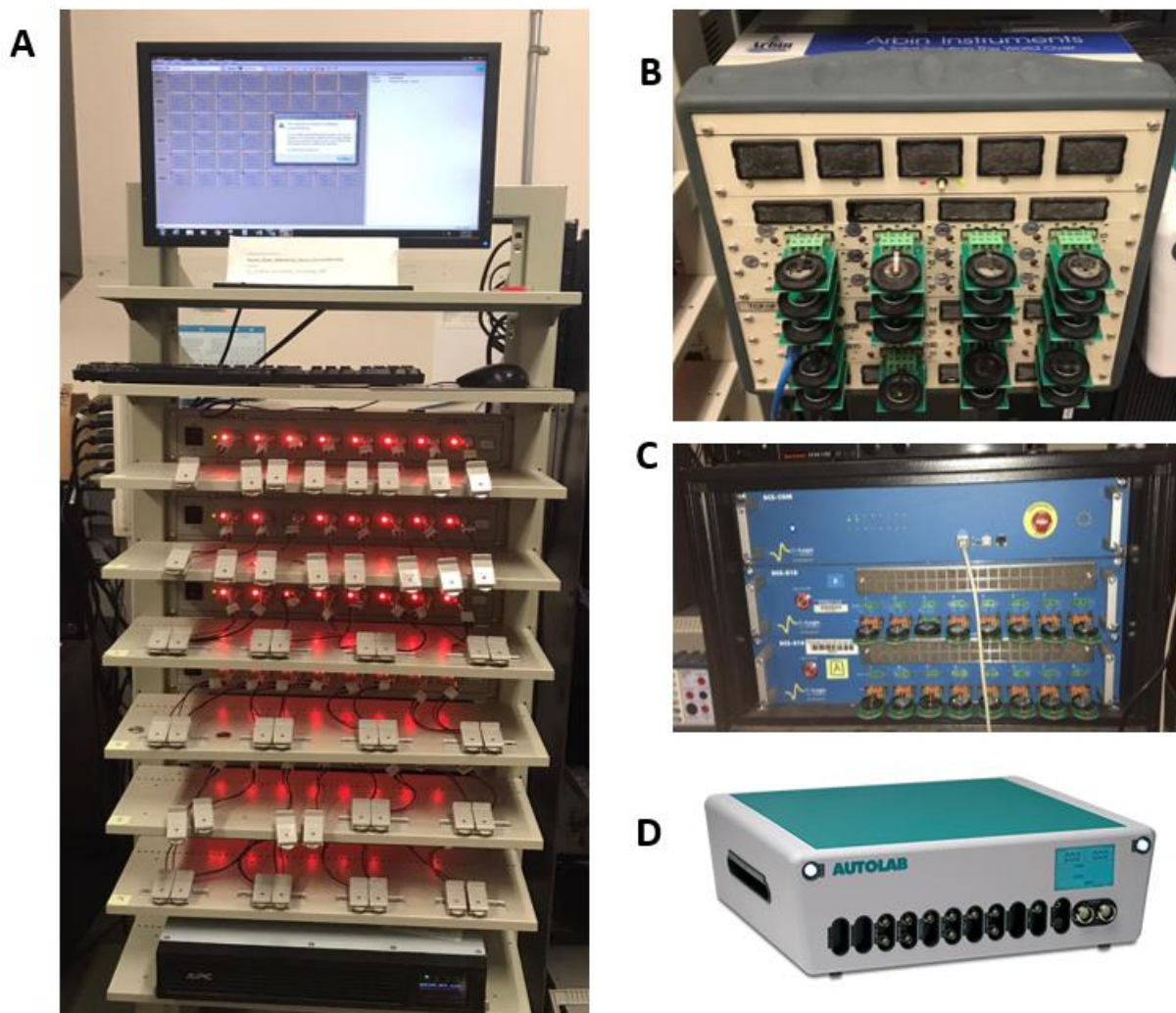


Figure 8. **A.** LANHE battery testing system (CT2001A). **B.** Arbin automatic battery cycler **C.** Biologic (MCS810). **D.** Metrohm Autolab

Galvanostatic charge and discharge experiments were performed using a LANHE battery testing system (CT2001A) over the same voltage range at room temperature using

charge/discharge rates of 100 and 200 mA g⁻¹. Li-ion half-cells were also tested using an Arbin automatic battery cycler to evaluate the rate performance at current densities of 50, 100, 200, 400, and 500 mA g⁻¹ between cut-off potentials of 0.01 and 3 V. The electrochemical impedance spectroscopy experiments were performed over the frequency range from 1 kHz to 0.005 Hz using a Metrohm Autolab (PGSTAT 128 N, Metrohm).

CHAPTER IV

EXPERIMENTAL PROCEDURE

3.1 Fabrication of Carbon Fibers from PAN

Carbon fibers (CFs) were prepared from PAN precursor fibers by dissolving 12 wt. % PAN in DMF. The solutions were stirred for 24 h using mechanical mixing to obtain homogeneous precursor solutions. Pristine PAN microfibers were obtained by centrifugal spinning at a rotational speed ranging from 6500-8000 rpm and relative humidity below 40% (Figure 1). The fibers were then collected on a rectangular aluminum substrate and subsequently dried under vacuum at 60 °C. After drying, the fibrous mat was stabilized in air at 280 °C in an OTF-1200X tube furnace (MTI Corp. California, USA) for 4 h (heated at a rate of 3 °C/min), which was followed by carbonization under argon atmosphere at 600 °C for 6 h.

3.2 Preparation of Co₃O₄-Coated Carbon Fibers

The Co₃O₄ coated carbon fibers (CCFs) were prepared by dispersing low concentrations of Co₃O₄ nano-powder into ethanol and stirring for 5 h. Subsequent to stirring, the mixture was sonicated for 1 h. The fibrous PAN mats were weighed and coated with 30, 50 or 70 wt.% of Co₃O₄ nanoparticles (CCF30, CCF50 and CCF70, respectively). The fibrous mats were placed flat on a surface where a proper amount of solution was poured and sonicated for 1 h. The samples were then dried at room temperature for 24 hours prior to heat treatment. In this process,

the coated fibers were placed in an OTF-1200X tube furnace, stabilized under air at 280 °C for 4 hours (at a rate of 3 °C/min), and carbonized under argon atmosphere at 600 °C for 6 hours.

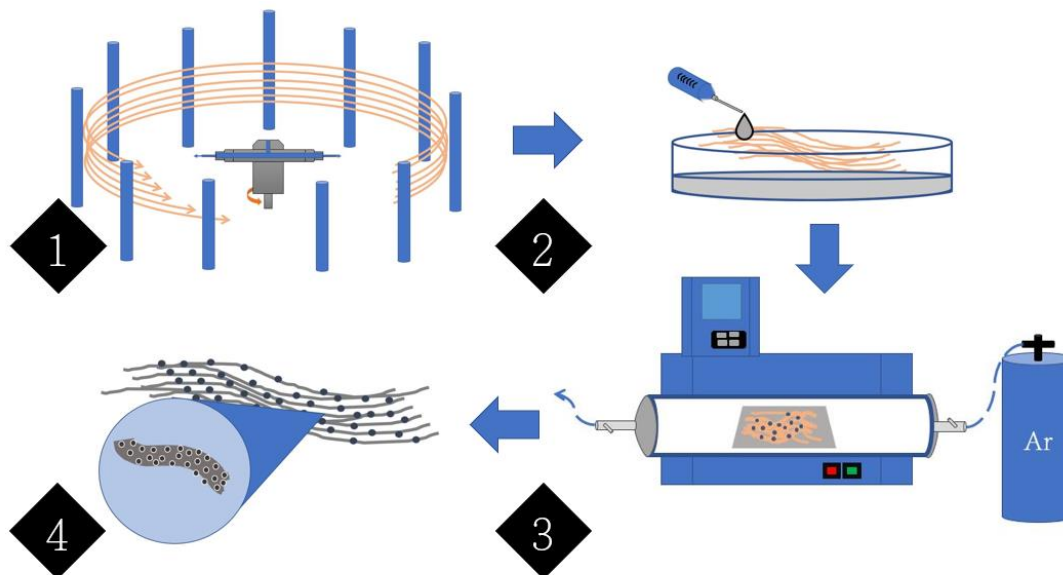


Figure 9. Schematic showing processing of composite fiber electrodes

3.3 Fabrication of Carbon Fibers from PVP

Carbon fibers were prepared from PVP precursor solution by dissolving 15 wt % PVP in Ethanol. The solutions were stirred for 24 h using mechanical mixing to obtain homogeneous precursor solutions. Pristine PVP fibers were obtained by centrifugal spinning using rotational speeds ranging from 7000-8000 rpm and relative humidity below 50%. The fibers were collected on a rectangular aluminum substrate and dried under vacuum at 60 degrees to remove humidity. After drying, the fibers were then annealed in air at 160 °C in a Carbolite Gero (CWF 1300) oven. After 24 hours, the fibers were removed from heat, and allowed to return to room temperature before proceeding to heat treatment using 2°C /min ramp rate and a carbonization temperature of 750 °C for 3 hours under inert gas.

3.4 Fabrication of Silicon/Carbon Fiber Composite Anodes

Silicon carbon fibers (SCFs) were prepared by dispersing 10% Si nanoparticles in solutions of 15 wt % PVP in Ethanol. After the addition of silicon, the solutions were left to stir for 48 hours, using mechanical mixing to obtain proper dispersion of nanoparticles. Pristine Silicon/PVP fibers were obtained by centrifugal spinning using rotational speeds ranging from 7000-8000 rpm and relative humidity below 50%. The fibers were collected on a rectangular aluminum substrate and dried under vacuum at 60 degrees to remove humidity. After drying, the fibers were then annealed in air at 160 °C in an Carbolite GERO furnace (CWF1300). After 24 hours, the fibers were removed from heat, and allowed to return to room temperature before proceeding to heat treatment using an OTF-1200X tube furnace (MTI Corp. California, USA) 2°C /min ramp rate and a carbonization temperature of 750 °C for 3 hours under inert gas to prevent increased oxidation of silicon nanoparticles. A portion of SCFs (SiCFCMC). Were treated by dip coating in a solution containing 10 wt% NaCMC in deionized water for 10 minutes, followed by drying under vacuum at 40 °C for 24 hours.

3.5 Fabrication of Silicon Slurry Anodes

Silicon slurry anodes were prepared via mechanically stirring of the three main components: Silicon as the active material (AM), Carbon Black and Carbon Fibers as Conductive Additive (CA), and CMC, Na-CMC as binder (B). The ratios used to show in this work were determined from weeks work varying ratios to find a good electrochemical performance and ended up being optimal at a ratio of (27:36:36) AM:CA:B. The conductive filler was varied in the form of carbon black, carbon fibers, as well as the incorporation of metal

oxide fibers of Co_3O_4 and TiO_2 derived from centrifugally spun fibers followed by oxidation (150°C for Co_3O_4 and 500°C for TiO_2). Table 1 summarizes the different slurries made as well as their components. However, only the best slurries are shown and discussed in chapter V.

Table 1: Components of processed silicon slurry anodes

ID	(AM:CA:B)	Conductive Filler	Binder
Slurry 1	80:12:8	Carbon Black	CMC
Slurry 2	80:12:8	Carbon Fiber	CMC
Slurry 3	50:20:30	Carbon Black	CMC
Slurry 4	50:20:30	Carbon Fiber	CMC
Slurry 5	40:40:20	Carbon Black, Carbon Fiber (1:1)	CMC
Slurry 6	30:40:30	Carbon Black, Carbon Fiber (1:1)	CMC
Slurry 7	30:30:40	Carbon Black	CMC
Slurry 8	30:30:40	Carbon Black	Na-CMC
Slurry 9	30:30:40	Carbon Black, Carbon Fiber (1:1)	CMC
Slurry 10	27:36:36	Carbon Black, Carbon Fiber (1:1)	CMC
Slurry 11	27:36:36	Carbon Black, Carbon Fiber (1:1)	Na-CMC
Slurry 12	27:36:36	Carbon Black: Porous Carbon Fiber (1:1)	Na-CMC
Slurry 13	27:36:36	Carbon Black: CNT/Carbon Fibers (1:1)	Na-CMC
Slurry 14	27:36:36	Carbon Black: $\text{Co}_3\text{O}_4/\text{C}$ Fibers (1:1)	Na-CMC
Slurry 15	27:36:36	Carbon Black: TiO_2/C Fibers (1:1)	Na-CMC

3.6 Electrochemical Evaluation Tests

Before use in the Li-ion half cells, all anodes were dried under vacuum at 60 °C overnight to prevent moisture in the sample. The anodes were weighed and placed into a MBRAUN (LABstar-pro) glove box filled with ultra-high purity argon with H₂O and O₂ concentrations of <0.5 ppm. They were assembled using CR2032 coin cells by employing a lithium chip as the counter electrode. Cyclic voltammetry (CV) experiments were performed using Biologic (MCS810) at a scan rate of 0.2 mVs⁻¹ at a range from 0.01 to 3.0 V (vs Li/Li⁺). Galvanostatic charge and discharge experiments were performed using a LANHE battery testing system (CT2001A) over a range of 0.01 – 3.0 V at room temperature using charge/discharge rates of 100. For the slurry anodes, the weight of the copper was subtracted in order to take into account only the dry weight of the electrode. The electrochemical impedance of all Li-ion half cells was measured with a Metrohm Autolab (PGSTAT 128 N, Metrohm)

CHAPTER V

RESULTS AND DISCUSSION

4.1 Morphology and Characterization

4.1.1 Carbon Fibers (CFs) & Composite Co₃O₄/C Fibers (CCFs)

Figure 10 shows SEM images of CFs and CCFs after carbonization of the precursor fibers. The fiber diameter distribution (histograms) of CFs and CCFs are also shown in Figure #. The average fiber diameter of the CFs was approximately 1 μm , while the diameter of the CCFs was between 1.5 and 2 μm . The presence of agglomerated nanoparticles on the surface of the PAN fibers may have prevented some loss of mass as can be observed with the increase in diameter compared to the uncoated samples (CF). Alternatively, the Co₃O₄ NPs on the surface may be partially embedded into the CFs, which would cause an increase in the fiber diameter compared to the pristine CFs. The SEM images in Figure # show a good dispersion of Co₃O₄ nanoparticles on the carbon fibers. To avoid moisture in the atmosphere from being absorbed by the metal-oxide nanoparticles, the Co₃O₄ NPs were stored in a large desiccator prior to mixing with ethanol. The low concentration of nanoparticles enabled uniform coating on the surface of the PAN fibers, although some agglomeration of the Co₃O₄ NPs on the fiber surface was apparent at higher Co₃O₄ concentrations nearing 60 wt%. The surface defects on the fibers, which can be observed in Figure 2 (B), may have helped the cobalt nanoparticles adhere to the surface of PAN fiber.

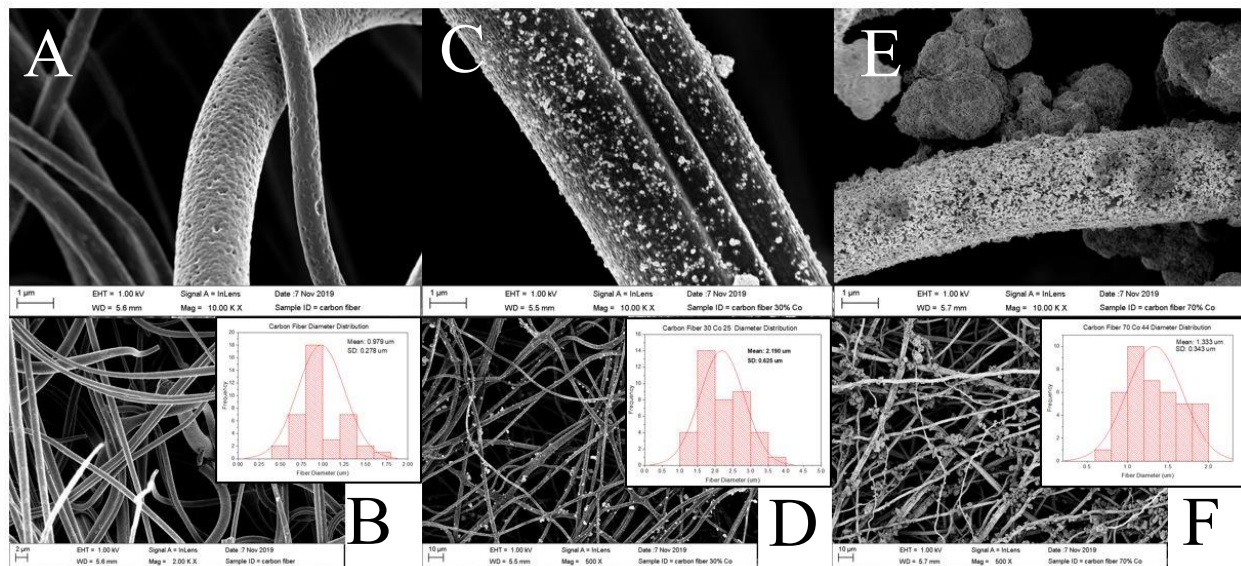


Figure 10. A. SEM and size distribution of CF anode electrodes at 10,000X. B. 5,000, Co₃O₄/C. C. Composite Fibers at 10,000X, D. 5,000 X. E. a higher concentration Co₃O₄/C Composite Fibers at 2000X, and F. 5,000 X magnifications. Inserts show the fiber diameter distribution (histograms).

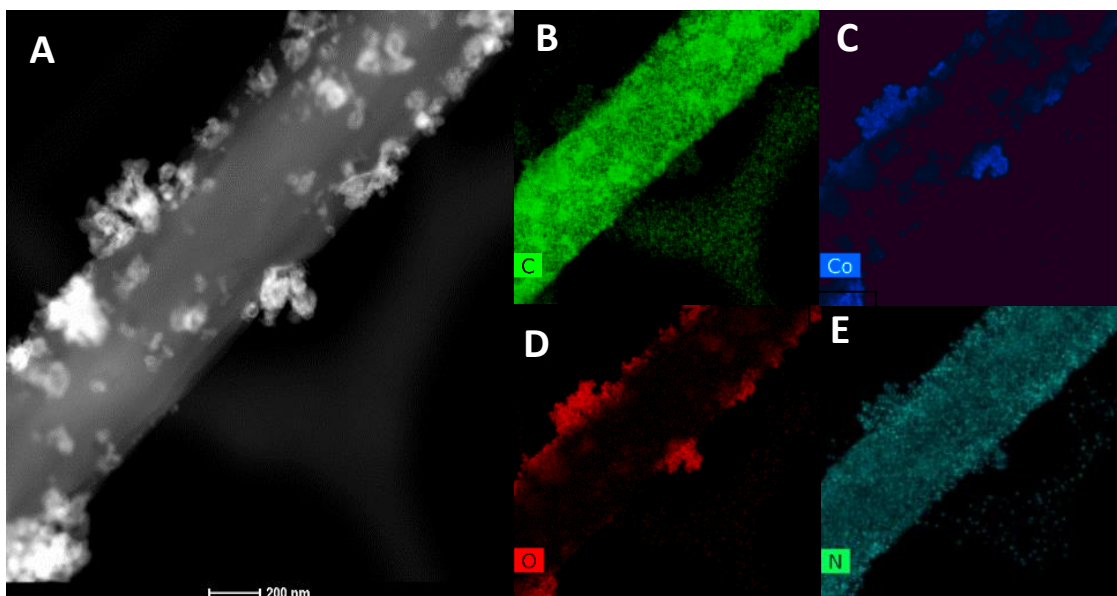


Figure 11. HRTEM image of Co₃O₄ nanoparticles embedded in carbon fibers. B. Carbon, C. Cobalt D. Oxygen, E. Nitrogen of the Co₃O₄/C composite fibers.

Figure 11 C shows the presence of both the carbon fibers and Co₃O₄ nanoparticles close to the carbon-fiber matrix, while some nanoparticles are embedded in the fibers. In addition,

some carbon fibers show graphitic character, which is represented by the alignment of the atoms in the structure. The EDS mappings and bright field images of the $\text{Co}_3\text{O}_4/\text{C}$ composite fibers are shown in Figure 11 (B-E). It can be observed in Figure 11 (B-E) that the CCFs sample consists of carbon, nitrogen, oxygen, and cobalt. The EDS mappings of the carbon and nitrogen correlate closely with one another, which is consistent with using PAN as the carbon source. The light carbon present in the background of the EDS mapping (Figure 11 B) is due to the carbon-coated grid used for the TEM. In addition, the sample was carbon-coated for the TEM data collection and analysis. Furthermore, there is a high correlation between the presence of Co and O in the EDS mappings, confirming a cobalt oxide structure. However, there is also a correlation among the positions of the O, N, and Co in the elemental maps. The elevated N concentrations from the carbonized PAN fibers correlate to the positions of high concentrations for both Co and O in the sample. This might indicate that the existence of residual N in the PAN fibers after carbonization was the point of attachment or bonding for the Co_3O_4 nanoparticles. In addition, the presence of N in proximity to the CoO nanoparticles may help explain the observed reduction of Co_3O_4 to a combination of Co metal and CoO. The lone pair of electrons on N may have been used to reduce the Co_3O_4 during the carbonization process and then contribute to a stronger bond between the $\text{Co}_3\text{O}_4/\text{Co}/\text{CoO}$ and the fibers.

Desired concentrations of Co_3O_4 on carbon fibers were approximated using calculations prior to coating, however, to find the true concentration of cobalt oxides in the samples, Thermogravimetric Analysis was performed on all concentrations of composites and on carbon fibers. Figure 12 shows TGA thermograms of carbon fibers (CF), and composite fibers CCF30, CCF50, and CCF70. The experiments were performed under air atmosphere over a temperature range between 25 and 900 °C at a heating rate of 10 °C min^{-1} . A 5% weight loss was observed

for all CCF samples at a temperature below 200 °C, while a 10% weight loss was observed for CFs. This initial loss is attributable to the removal of water from the samples. The cobalt oxide content in the fibers correlates well with that used in the precursor solutions to prepare the Co₃O₄-coated PAN fibers. It can be observed in Figure 6 that the residual mass in the CF, CCF30, CCF50 and CCF70 samples is 5, 27, 50 and 60 wt. %, respectively

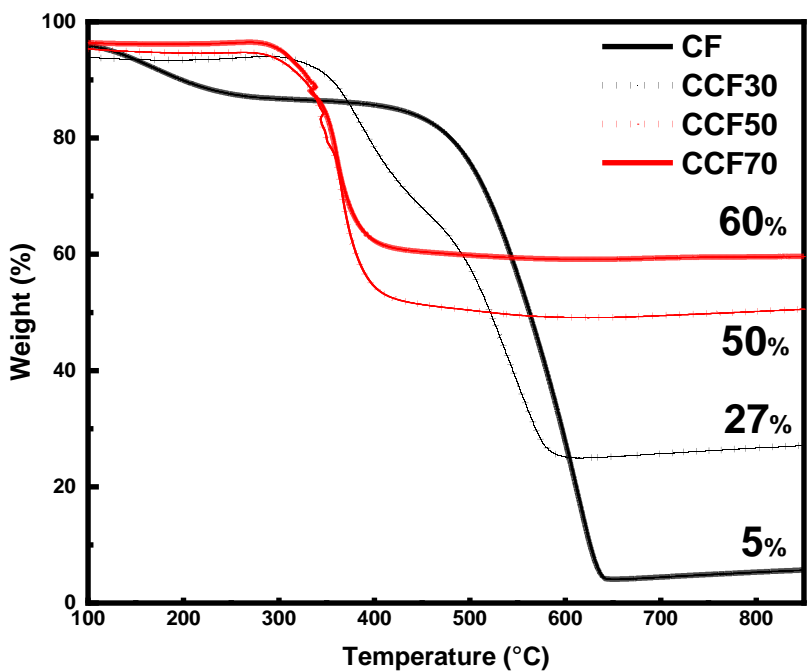


Figure 12. TGA curves of CF, CCF30, CCF50, and CCF70 samples, obtained at 10 °C min⁻¹

4.1.3 Silicon/Carbon Fiber Composite Anodes

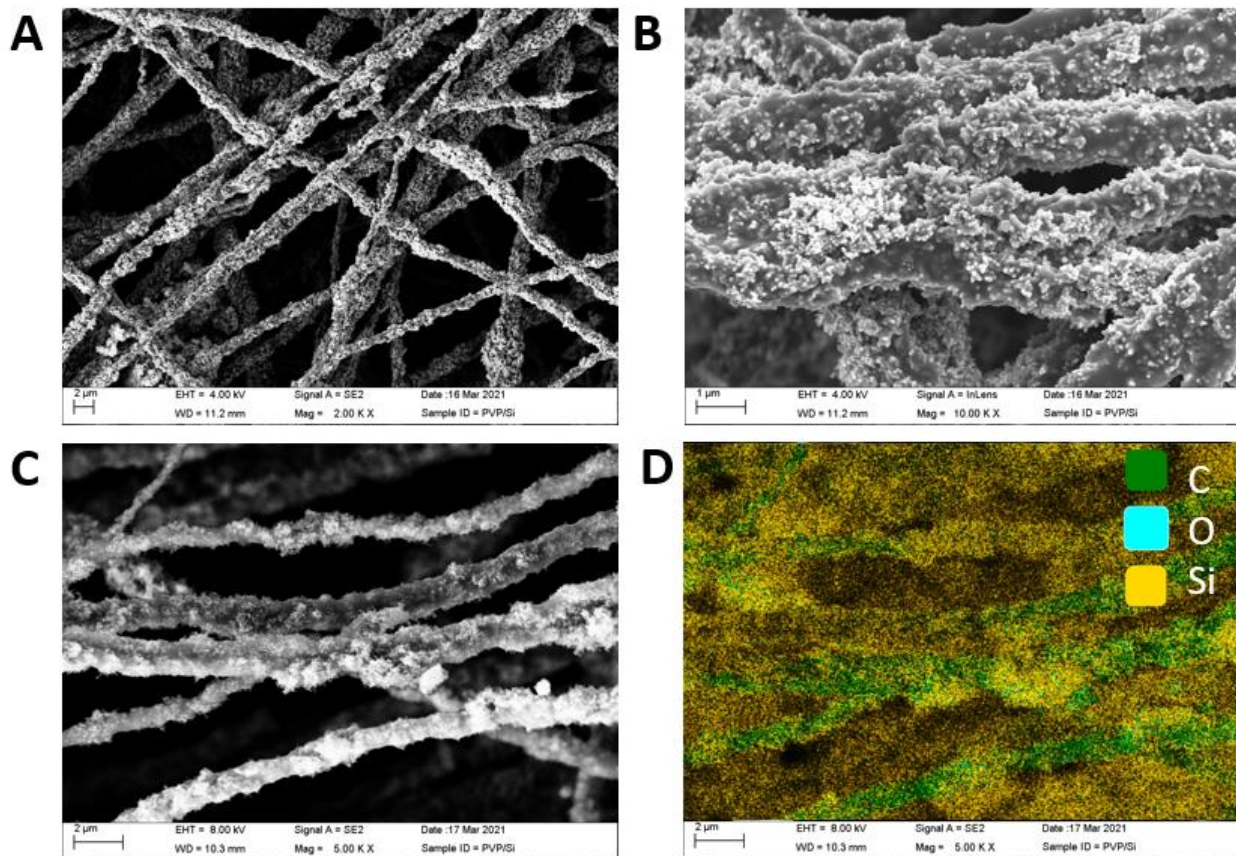


Figure 13. **A.** SEM images of fiber anodes from carbonized Si/PVP fibers. **B.** In-lens image at high magnification of carbonized Si/PVP fibers. **C.** SEM image used to probe EDS maps. **D.** EDS maps of fiber anodes from carbonized Si/PVP fibers.

Figure 13 shows SEM images at 2K and 10K magnifications, and EDS Map of Silicon/Carbon Fiber Composite Anode (D) with its respective SEM image (C). The composite fibers were derived from Centrifugally spun Si/PVP. Images and EDS maps were collected post heat treatment, which can be seen in figure 13 D, as mainly carbon fibers and Silicon are present in the samples.

4.1.3 Surface Morphology and Characterization of CMC Coated Silicon/Carbon Fiber Composite Anodes

Figure 14 shows SiCF's after heat treatment and after coat-processing. The presence of silicon agglomerations can be observed at the surface of the carbon fibers. CMC is known to form covalent bonds with the native oxide layer in silicon particle surfaces, which were likely the bonding place for the CMC coating films. Although some webbing CMC films can be noticed between the fibers, these CMC coatings are believed to have played a significant contribution to the diminished effect of the SEI layer when compared to Silicon/Carbon fiber composites that were not treated with CMC.

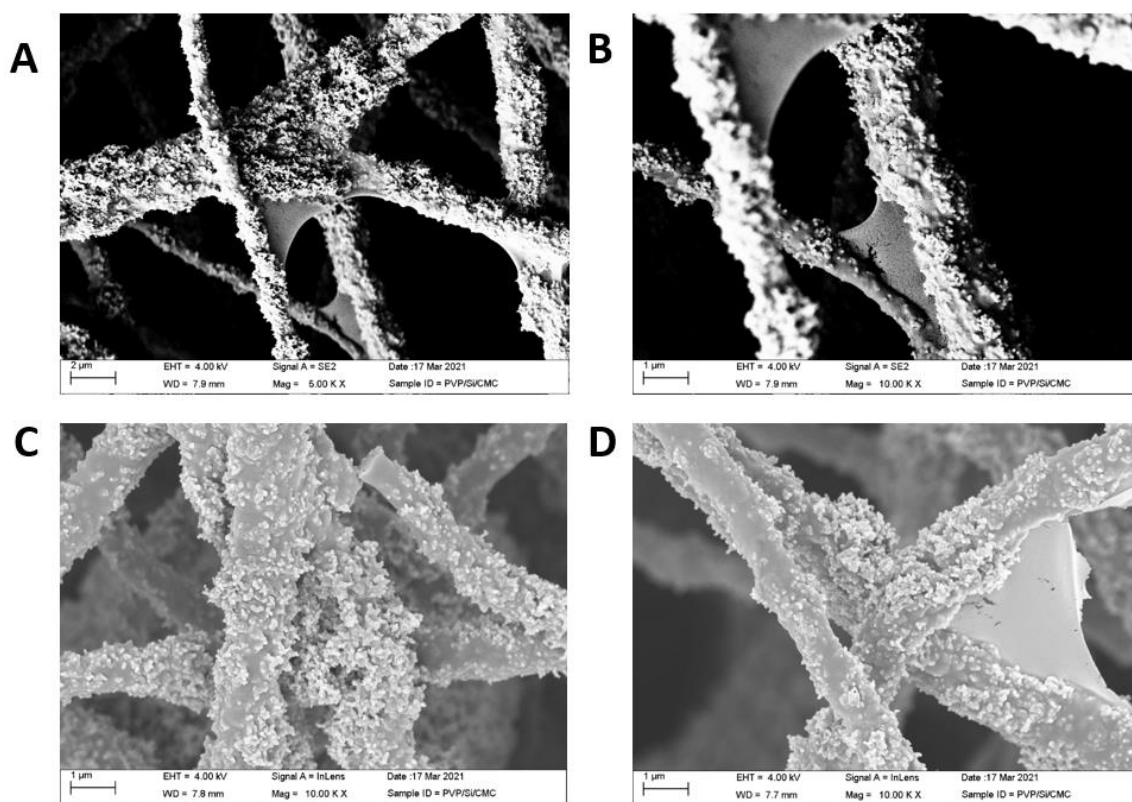


Figure 14 A. SEM images of fiber anodes from carbonized Si/PVP fibers coated with CMC. B. In-lens image at high magnification of carbonized Si/PVP fibers coated with CMC. C. SEM image at high magnifications. D. In-lens SEM image at high magnification.

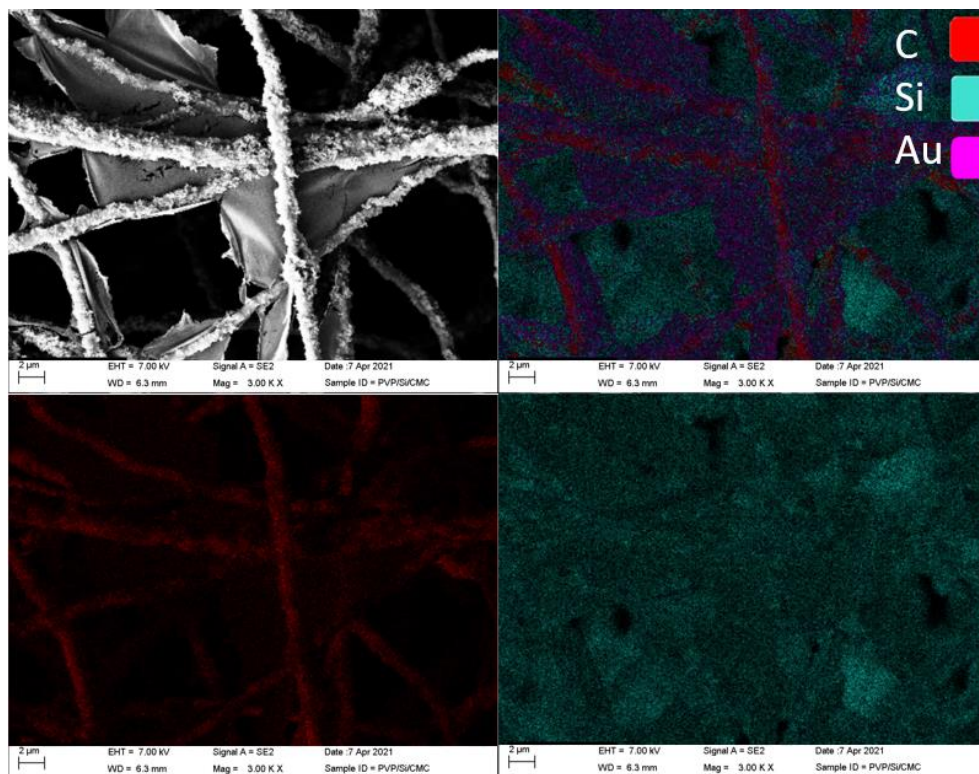


Figure 15. EDS Mapping of silicon carbon fiber anodes coated with Na-CMC, sputter coated with Gold.

EDS Mappings show the presence of silicon in the carbon fiber composite, as well as carbon dispersed in the CMC films. Furthermore, X-ray Photoelectron Spectroscopy was used to investigate the bonding environments present in the fiber electrodes prior to electrochemical cycling. Figure 15 shows C1s scans of the PVP/Si after heat treatment which consisted of annealing at 160 for 24 hours, and heat treatment under argon at 750 °C. The C1s scan of both samples shows the presence of the C-C bond, as well as a small peak corresponding to the C-N due to the nitrogen in the PVP. However, for the sample coated with CMC after heat treatment, a peak observed near 287 eV was attributed to the C-O bonding of the Na-CMC with the oxide surface layer of the silicon particles [52, 53]. Si2p scans show the presence of SiO₂ likely formed in the annealing step. Little difference is seen on the samples coated with CMC in

deionized water which was believed to have played a role in the oxidation into SiO₂. The presence of Si and SiO peaks are similar to those found in the literature [52, 54].

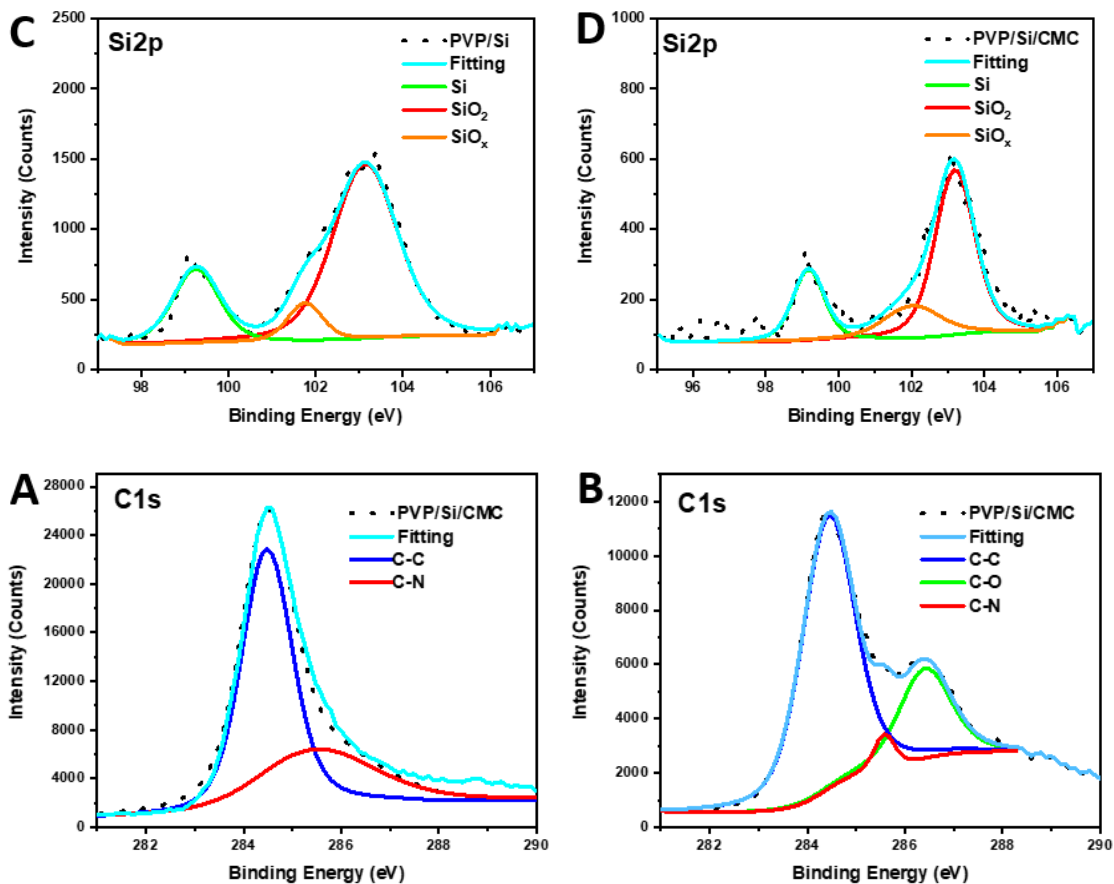


Figure 16 XPS C_{1s} scans of **A.** PVP/Si and **B.** PVP/Si/CMC and Si_{2p} scans of **A.** PVP/Si and **B.** PVP/Si/CMC

4.1.4 Silicon Slurry Anodes

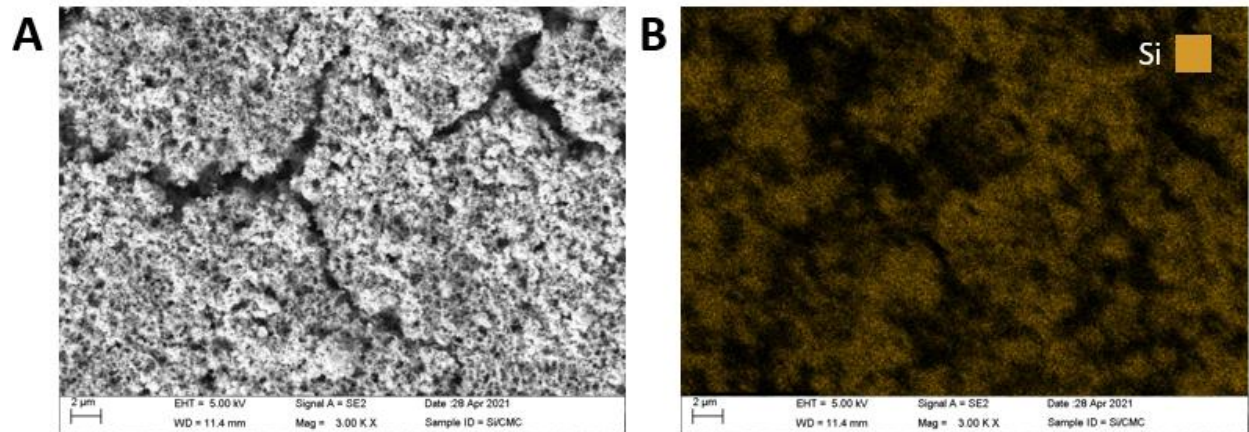


Figure 17 A. SEM image of silicon slurry anodes. **B.** EDAX Mapping of silicon composition

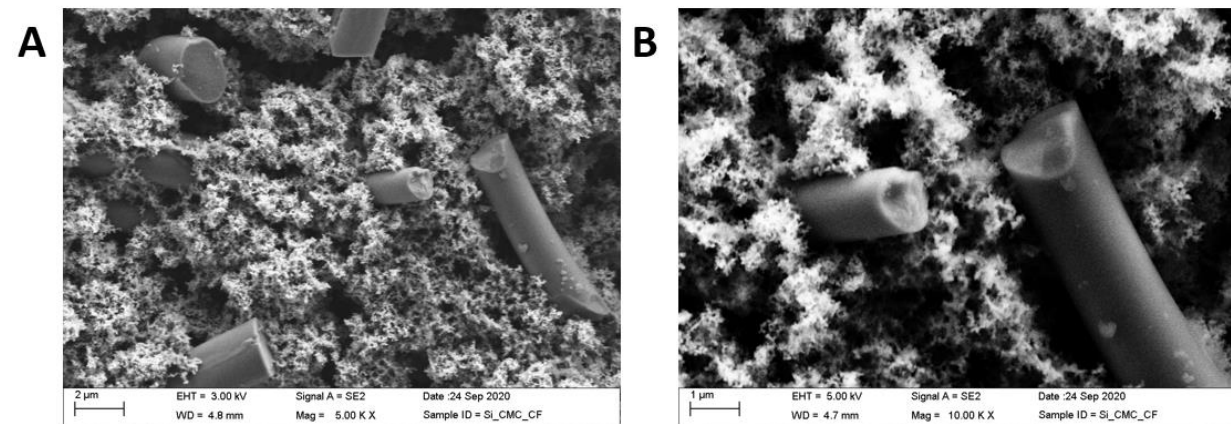


Figure 18 A. SEM image of silicon/carbon fiber slurry anodes. **B.** SEM image of silicon/carbon fiber anodes at high magnification.

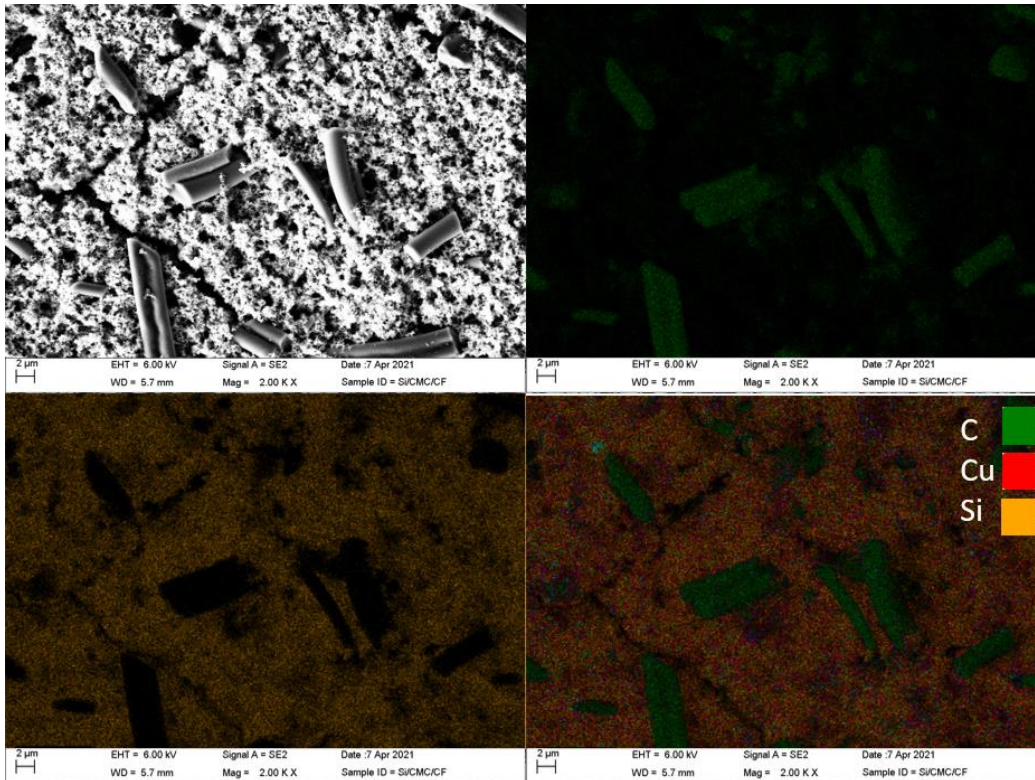


Figure 19: EDS Mapping of silicon slurry anodes with carbon fiber as conductive additive.

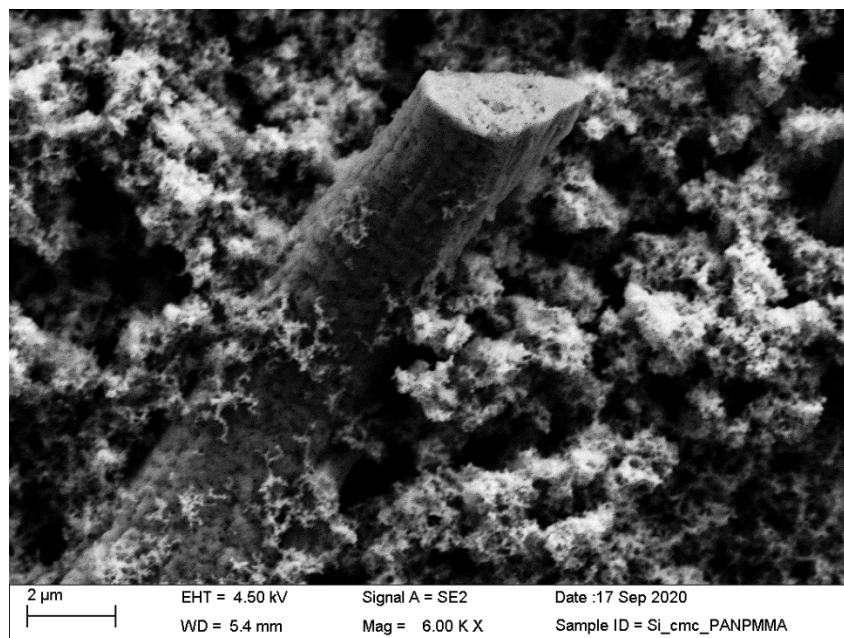


Figure 20 SEM image of silicon/porous carbon fiber slurry anodes derived from PAN/PMMA fibers after carbonization.

Figure 18 SEM images show the incorporation of sort carbon fibers derived from centrifugally spun PVP (slurry 11 in Table 1), and the mapping of EDS showing the presence of the carbon fibers in the silicon electrodes in figure 19. In addition, figure 20 shows the use of porous carbon fibers derived from centrifugally spun PAN/PMMA (Slurry 12 in Table 1), as conductive additives in a silicon slurry anode with CMC as binder. These fiber anode electrodes showed good electrochemical performance (800 mAhg^{-1}) for PVP, and 600 mAhg^{-1} for porous PAN/PMMA.

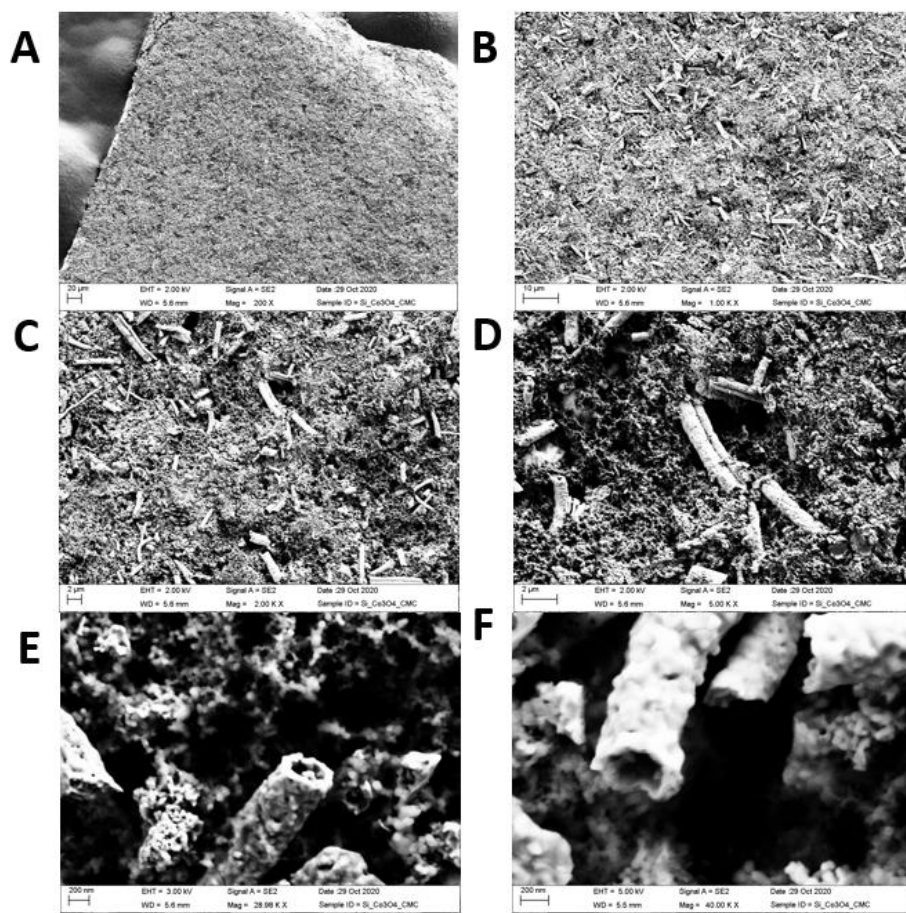


Figure 21 SEM images of Co₃O₄ short fibers imbedded in silicon slurry anodes

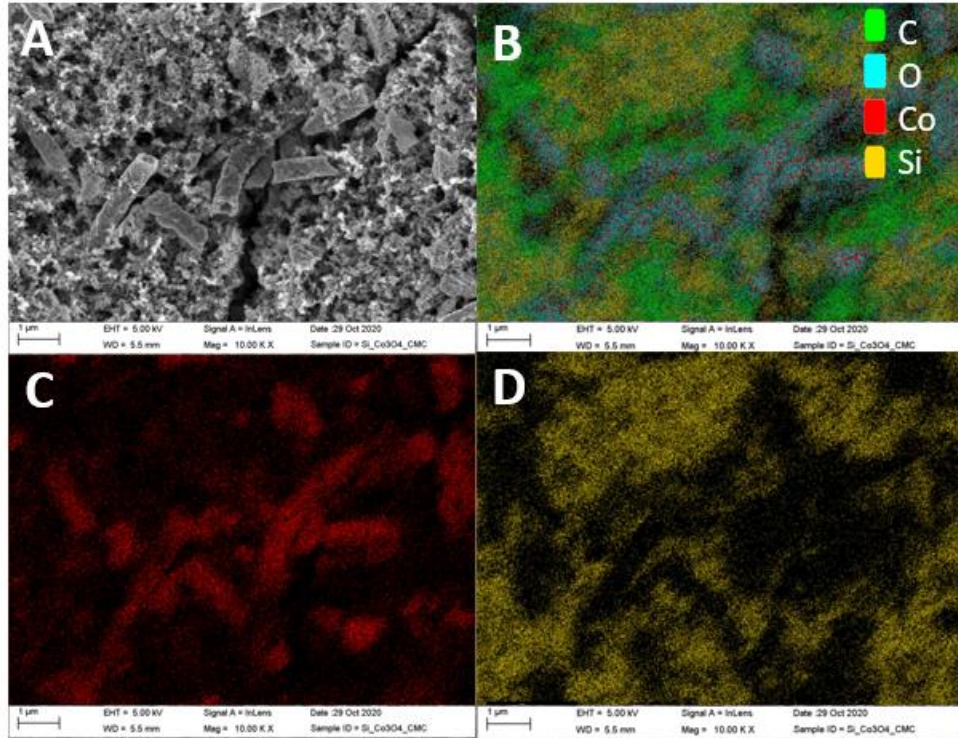


Figure 22 EDS Mapping showing Co_3O_4 short fibers imbedded in silicon slurry anodes **B** Elemental Overlay **C**. Cobalt Map **D**. Silicon Map

Figure 21 & 22 show SEM images of Co_3O_4 short fibers with good dispersion imbedded in silicon slurry with CMC as binder. (Slurry 14 in Table 1). The presence oxygen in the fibers confirms the oxidation of cobalt precursor to form cobalt oxide during the heat treatment. Cobalt oxide fibers can be seen in the EDS maps, which confirms the presence of the cobaltous fibers within the silicon slurry anode.

4.2 Electrochemical Results

4.2.1 Carbon Fibers & Co₃O₄/Carbon Fiber Composite Anodes

Figure 23 shows cyclic voltammetry (CV) results of CF (A) and CFF70 (B) composite electrodes during the first four scans at a rate of 0.2 mV s^{-1} . It is observed in Figure 7A that the carbon-fiber electrode shows obvious cathodic peaks close to 0.75 V and anodic peaks at ca. 0.35 V , corresponding to the Li^+ intercalation/deintercalation reactions. In the first cathodic scan (lithiation) of the CFF70 electrode (Figure 7B), a peak is observed at ca. 0.55 V which is assigned to the reduction of cobalt oxide species (CoO , Co_3O_4) into Co [55-57]. This reduction peak was shifted to lower voltage in the subsequent cathodic scans indicating the occurrence of some irreversible reactions, such as those of cobalt oxide with lithium ions to form Li_2O [31, 58, 59]. The intensity of this oxidation peak decreases during the subsequent anodic scans.

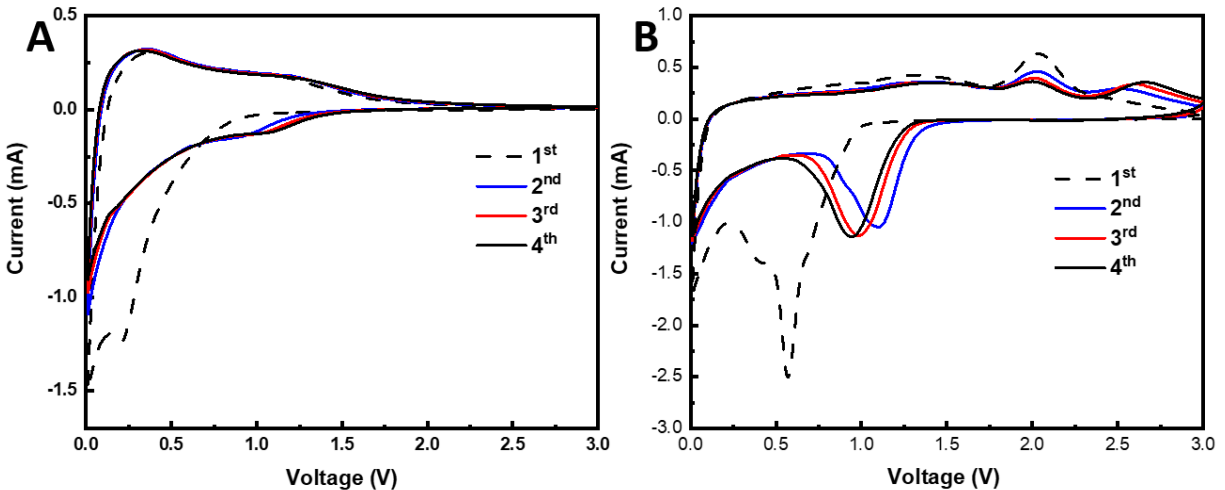


Figure 23 A. Cyclic voltammetry of CF and CFF50 B. in a half-cell configuration and cycled between 0 and 3.0 V at a scan rate of 0.2 mV s^{-1} .

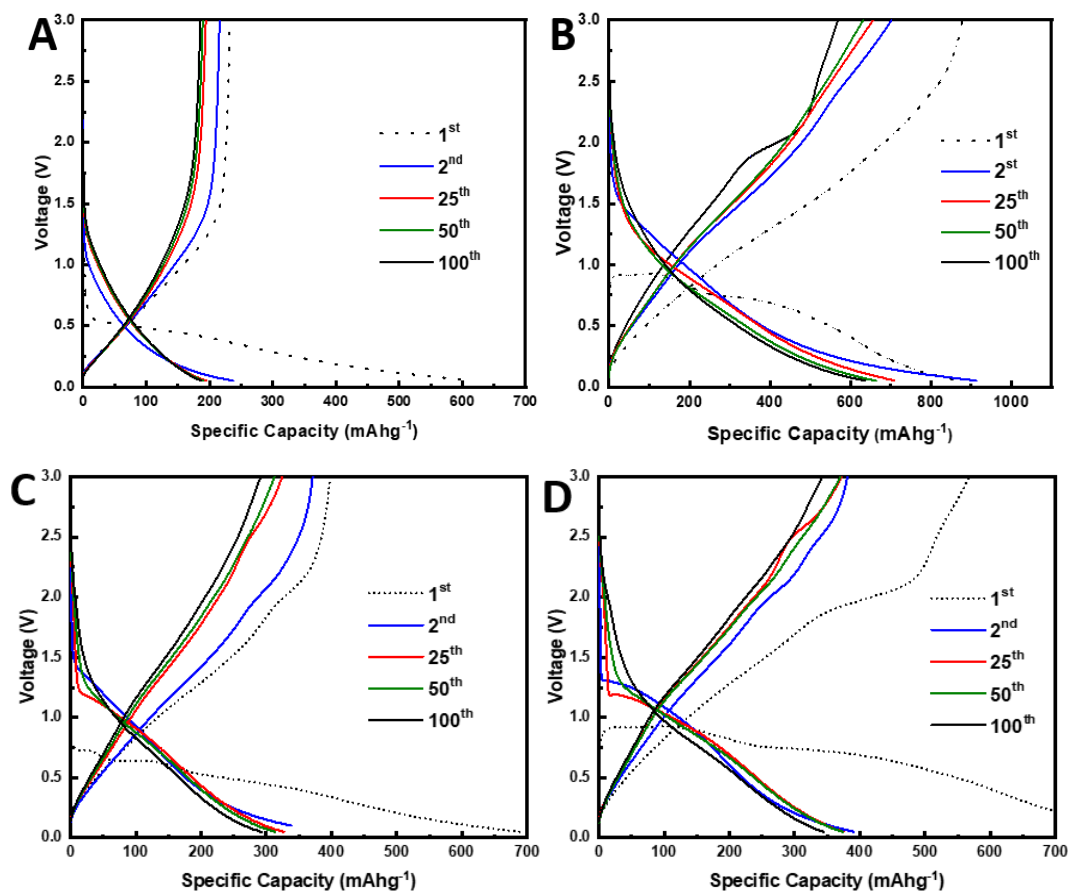


Figure 24 Galvanostatic charge/discharge profiles of **A.** CF, **B.** CCF50 at 100 mA g^{-1} , and **C.** CCF30(C), **D.** CCF70(D) at 200 mA g^{-1} at a cut-off voltage between 0.1 and 3V.

The charge-discharge curves for carbon-fiber anodes with different concentrations of cobalt oxide (0, 30, 50, 70 %) are shown in Figure 24. During the first discharge cycle (lithiation), the anode potential drops to a voltage of less than 2 V (1.25 V for that charged at 200 mA g^{-1}) followed by long voltage plateaus observed in the range of 0.5-0.75 V. These voltage plateaus are characteristic of cobalt (Co_3O_4 and CoO) [36, 37]. The rapid initial loss in capacity from the first to 10th cycles can be attributed to the formation of a large SEI layer on the surface the composite-fiber anodes. It should be noted that the charge and discharge curves follow similar profiles after 10 cycles. The CCF composite anodes exhibited specific capacities of 625 mAh g^{-1} (CCF50) at 100 mA g^{-1} , and 300 mAh g^{-1} (CCF30), 420 mAh g^{-1} (CCF70) when cycled at 200 mA g^{-1} (Figure

24 C, D). The results indicate good stability of all CCF anodes with Co_3O_4 content up to 70 wt%. Additionally, there was a loss in specific capacity at increasing cycle number, which can be due to the high-volume change upon cycling as well as to the side reactions of lithium with oxygen to form LiO_2 . Despite some losses in capacity and coulombic efficiency at the first cycle, the CCF electrodes show almost double the specific capacity (Figure 24 B) of that for the pristine carbon-fiber anode (Figure 24 A). At a current rate of 200 mA g^{-1} and lower Co_3O_4 concentrations (CCF30), the composite-fiber electrodes still deliver a higher capacity when compared to carbon fibers.

Figure 21 A shows the cycle performance of CF and CCF composite anodes evaluated after 100 cycles at 200 mA g^{-1} . The breakdown and solidification of the electrolyte at the anode/electrolyte interface during the first discharge cycle is reflected in the loss of charge capacity after the first cycle (Li-deintercalation + conversion). This effect is amplified by the large surface area of the micro-fibrous mat, which contributes to the SEI formation at the first discharge cycle, resulting in a high irreversible capacity. However, the specific reversible capacity of carbon fibers remained stable after 100 charge/discharge cycles, suggesting that a good cyclability was observed for the CF and CCF anodes. After 100 cycles, the CCF30 delivered a slightly higher specific capacity than that of CF anodes (300 mAh g^{-1}) while CCF70 showed a specific capacity of 420 mAh g^{-1} after 100 cycles.

The rate performance results (charge capacity vs. cycle number) of CF and CCF anodes cycled at 50, 100, 200, 400, and 500 mA g^{-1} are shown in Figure 25 B. The performance of CCFs showed good cycling stability, and higher specific capacity when compared to the carbon fibers (CFs). At low current rates, the effect of the Co_3O_4 concentrations on the rate performance of the CCF composite electrodes is observed in the large gap in specific capacity where the higher

concentration of active material resulted in a higher capacity of the composite anode. However, at higher charge/discharge rates, increasing the concentration of active material did not yield a significant improvement in specific charge capacity of CFF anodes. When cycled at the original charge rate of 50 mA g^{-1} , the CF and CFF anodes delivered similar capacities to that at the first rate of 50 mA g^{-1} , indicating good capacity retention and stability of the anodes after charging/discharging at higher rates.

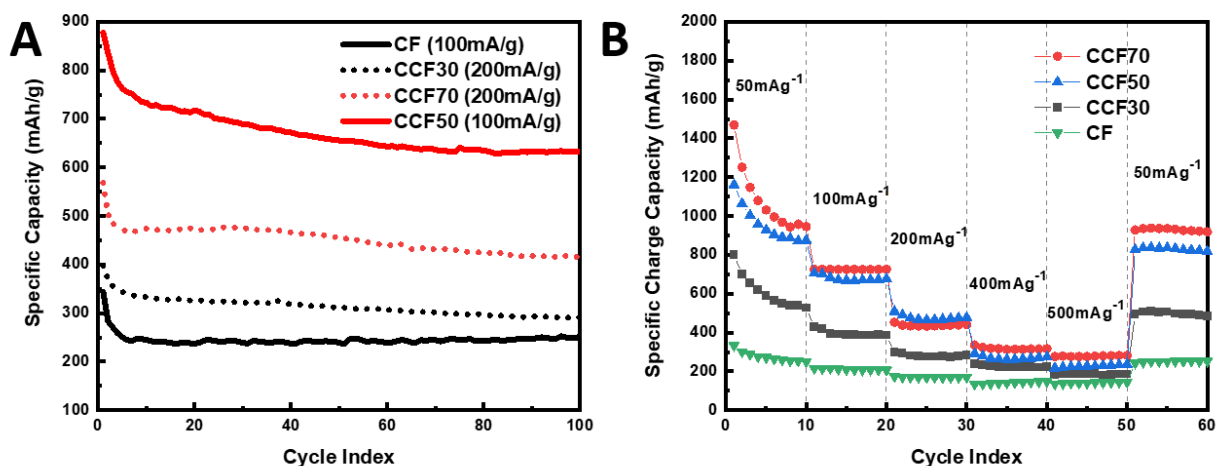


Figure 25 A. Cycle performance of CFs and CCFs at a charge/discharge rate of 200 mA g^{-1} B. Rate performance of CF, CCF30, and CCF70 in Li-ion half cells.

Electrochemical impedance spectroscopy (EIS) experiments (Nyquist plot) were performed on the $\text{Co}_3\text{O}_4/\text{C}$ composite-fiber electrodes before and after cycling at 100 mA g^{-1} (Figure 26). The semicircle observed in the medium to high frequency range is associated with different electrochemical processes within the cell. These processes include the SEI formation, contact resistance between materials, and reduction of cobalt oxide on the surface of the carbon fibers. Figure 26 B shows tabulated results for the modeling of the EIS spectra. In the equivalent circuit model (Figure 26 B), R_s is the electrolyte solution resistance, R_p is the charge transfer resistance, W is the Warburg impedance of Li ion diffusion into the active material at low frequency, and CPE is the constant phase-angle element equivalent to the double layer

capacitance [60]. With the increase in cobalt oxide content, the diameter of the semicircle increased because of the increase in the contact resistance at the electrode/electrolyte surface. When compared to freshly assembled cells, the aged cells (post cycled) showed larger and incomplete semi-circles followed by a tail with a lower slope than that for the fresh cells. This indicates that a slower diffusion took place in the low frequency range after 100 cycles. Higher concentrations of active material in the carbon fibers led to faster diffusion in the low frequency range (after 100 cycles), which is attributable to the greater amount of active material trapped in the carbon fibers after lithiation. Similar EIS results have been reported previously for cobalt-oxide electrodes [61, 62].

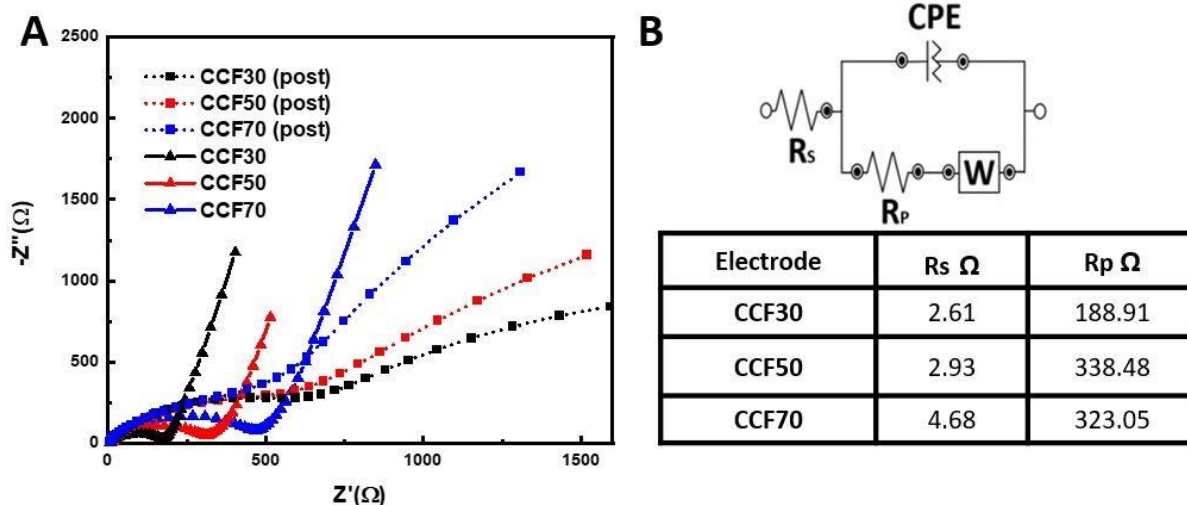


Figure 26 **A.** Electrochemical impedance results (Nyquist plots) of fresh and aged Li-ion half cells containing CCF electrodes with different Co₃O₄ constrictions. **B.** Impedance table showing R_s , R_p , and equivalent circuit model of the CCF anodes.

4.2.2 Silicon/Carbon Fiber Composite Anodes

The electrochemical performance for the PVP/Si and PVP/Si/CMC was evaluated by cyclic voltammetry and cycle performance and can be seen in figure 27. A portion of the experiments were tested with the addition of 10% FEC in the electrolyte. The first cathodic scan evolves four distinct peaks in figure A. The first two near 1.25 V and 0.60 V is associated to the initial reduction of the electrolyte, as well as the development of the SEI layer [63]. The cathodic peaks of subsequent cycles increase in intensity over four cycles, and the development of cathodic peak around 0.3V has been associated with the alloying voltages of lithiated phases of silicon. When coated with CMC (Figure C, D), the first cathodic scan does not show the peak near 1.25 which may indicate a protective effect provided by the CMC coating. Furthermore, the intensity of the cathodic peak near 0.6 V diminishes with the addition of CMC coating. Reduction peaks close to 0.01V, and 0.20V is seen in all figures likely due to the lithiation of carbon fibers and silicon, respectively. Anodic peaks located circa 0.45 – 0.5 V are associated with the del-lithiation of alloyed silicon phases. No peak shifts can be observed which indicates good reversibility. Similar CV results have been obtained for silicon and silicon oxide anode electrodes in literature. [64-66]

Cycle charge/discharge profiles are shown below in figure 28. The effects of both the FEC and the CMC on the fiber anode can be observed in the first two cycles. Without these two elements, the anode performs poorly (see figure 28 A), the initial discharge (lithiation) resulted in a lithiation capacity of 473 mAh/g and delivers a first charge capacity of 310 mAh/g. This accounts for a columbic efficiency of 65% in the first cycle. Similar results are obtained for fibrous anodes due to the large surface area and the formation of the SEI. With the addition of 10 % FEC additive in the electrolyte, the capacity of the anode increases to 1370 mAh/g in the first

cycle. This is seen in figure 28 B. Correspondingly, this anode delivers a charge capacity of the first cycle of 1141 mAh/g, accounting for an initial coulombic efficiency of 83%. Figure 28 C shows the charge discharge curves after the incorporation of CMC into the anode, tested without FEC. The results show that CMC coatings can enhance the capacity of the first cycle without the need for FEC. The first discharge capacity upon lithiation accounts for a specific capacity of 1752 mAh/g. The specific charge capacity corresponding to the first de-lithiation cycle was 1149 mAh/g, which accounts for a coulombic efficiency of 65%. This may suggest that CMC does increase specific capacity, however, does not have a significant effect increasing the first cycle coulombic efficiency. Figure D shows the charge discharge curves for CMC coated Si/CF anodes, tested with the addition of 10% FEC in the electrolyte. In the first discharge corresponding to the first lithiation of the anode, the uptake of ions results in a specific capacity of 3283 mAh/g more than twice the specific capacity of Si/CF in FEC and Si/CF/CMC without FEC. This anode delivered a charge capacity of 2747 mAh/g, corresponding to coulombic efficiency of 83%, likely a result of the addition of FEC.

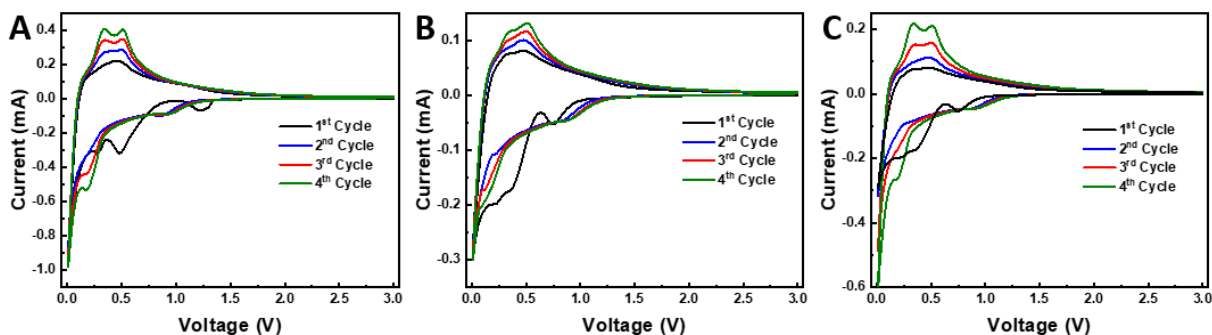


Figure 27. Cyclic Voltammetry of **A.** PVP/Si Electrode **B.** PVP/Si/CMC Electrode, and **C.** PVP/Si/CMC Electrode with 10% FEC additive in the electrolyte

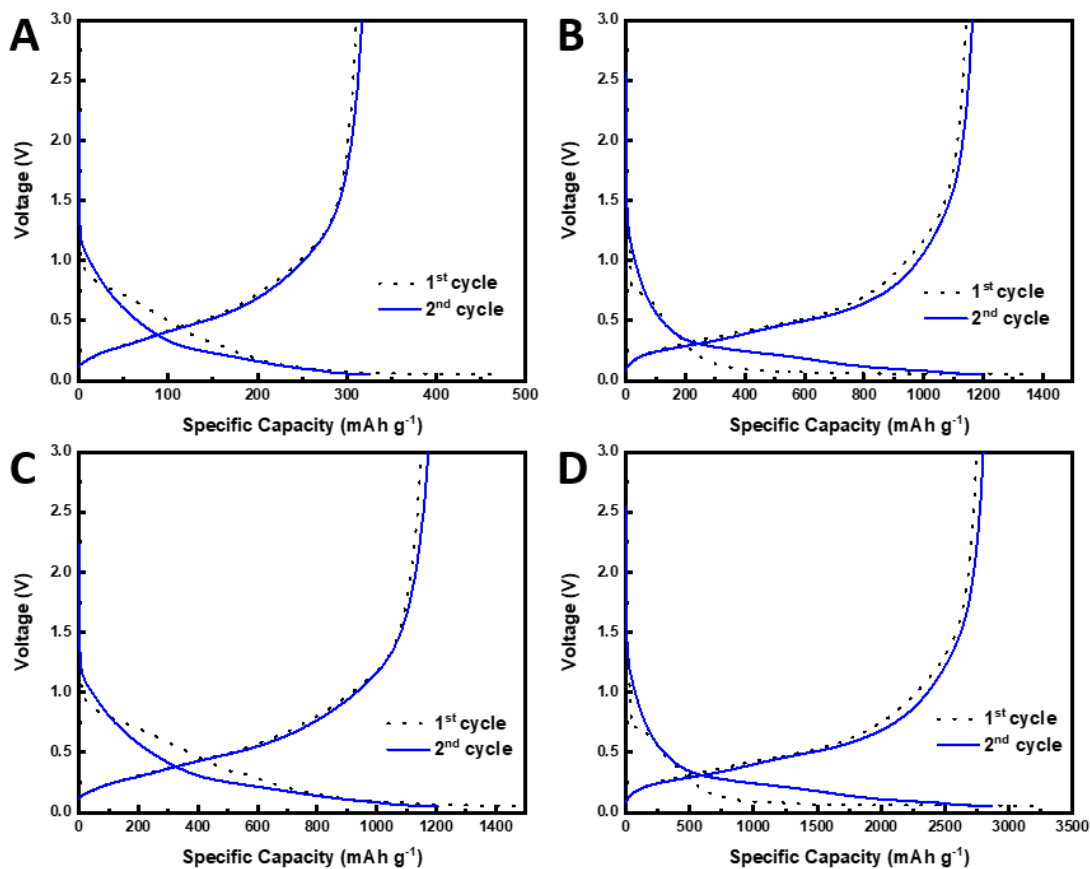


Figure 28 Cyclic Voltammetry of **A.** PVP/Si Electrode **B.** PVP/Si/CMC Electrode, and **C.** PVP/Si/CMC Electrode with 10% FEC additive in the electrolyte

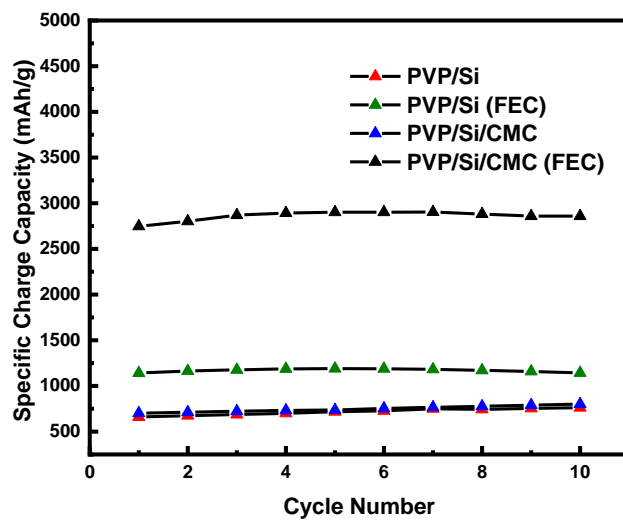


Figure 29 Charge Capacity (mAhg^{-1}) for 10 cycles for Silicon/ PVP Fiber electrodes

Figure 30 shows the electrochemical impedance spectroscopy for the silicon/pvp fiber electrodes and the Na-CMC coated silicon carbon fiber electrodes. Four samples were made when testing both with and without FEC. As seen in the figure, the addition of the CMC can increase the contact resistance between materials, due to the formation of a layer of polymer around the silicon fibers. Additionally, the FEC additive has similar film forming properties. The addition of both the Na-CMC and the FEC led to an increased resistance, however did provide better electrochemical performance.

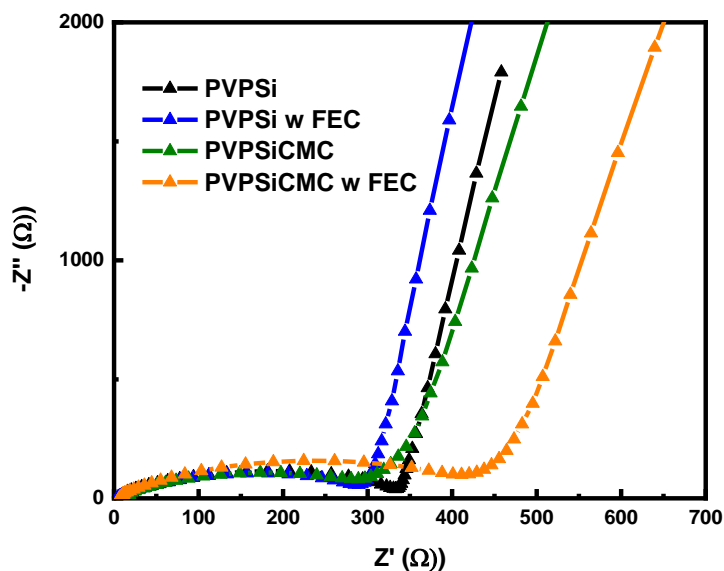


Figure 30 Electrochemical Impedance Spectroscopy of Silicon/ PVP Fiber electrodes

4.2.3 Silicon Slurry Anodes

The electrochemical results for silicon and silicon/carbon fiber slurries (slurries 9 and 11) are shown below. Figure 31, and 24. Figure 23 (A & B) show cyclic voltammetry of the silicon and silicon/carbon fiber slurries, respectively. The first cathodic peak is below 0.8 V and is often associated to the initial decomposition of the electrolyte and FEC additives, as well as the development of the SEI layer [63]. The cathodic peaks of subsequent cycles increase in intensity

over four cycles, and the development of cathodic peak around 0.3V has been associated with the alloying voltages of lithiated phases of silicon [64-66]. Reduction voltages in both slurry anodes are similar, however a larger cathodic peak close to 0.01V is seen in (B) likely due to the lithiation of the additional short carbon fibers. Anodic peaks located circa 0.45 – 0.5 V are associated with the del-lithiation of alloyed silicon phases. No peak shifts can be observed which indicates good reversibility. Similar CV results have been obtained for silicon and silicon oxide anode electrodes in literature.

Figure 31 C & D show charge/discharge profiles of silicon and silicon/carbon fiber slurries (slurries 9 and 11). The initial discharge capacity of the silicon and silicon/carbon fiber anodes are 1400mAhg^{-1} and 1300mAhg^{-1} , respectively. However, a loss of 35% is seen in the second discharge for both slurry anodes. This loss is associated with the formation of the SEI.

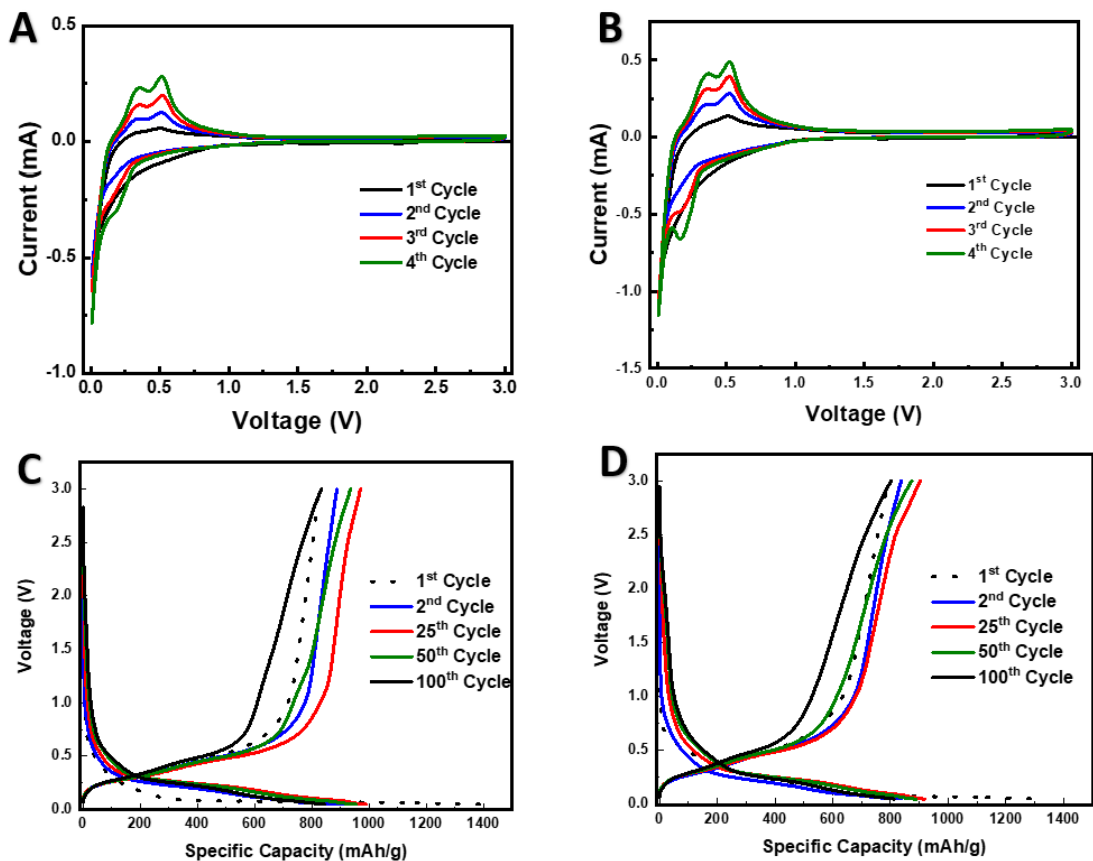


Figure 31. A. Cyclic Voltammetry of silicon slurry anodes. B. Cyclic Voltammetry of silicon/carbon fiber slurry anodes. C. Charge Discharge profiles of silicon slurry anodes. D. Charge Discharge profiles of silicon/carbon fiber slurry anodes.

To further investigate the slurry anode electrodes, cycle performance and electrochemical impedance spectroscopy was conducted. Figure 32 shows comparison between silicon and silicon/carbon fiber anodes (slurries 9 & 11), respectively. A similar yet slightly higher specific capacity (830 mAhg^{-1}) was observed for the silicon slurry anode composite after 100 cycles, however, slightly better cycle stability can be observed for the silicon/carbon fiber composite anode, delivering 802 mAhg^{-1} after 100 cycles at a charge rate of at 100 mA/g . This can also be observed in figure 32 A and B, where the specific charge capacity is plotted as a function of cycle number. EIS spectra comparing silicon and silicon/carbon fiber slurries are presented in figure

32 C. Similar spectra can be observed; however, a better diffusion of lithium-ions can be identified for the silicon slurry which shows a higher slope in the low frequency range.

Lastly, the addition of the short carbon fibers to the brittle- Na-cmc polymer binder may have served to reinforce the brittle structure and maintain structural rigidity as seen reflected in the better cycle stability. Additionally, the carbon fibers may have helped by increasing the theoretical capacity of the composite electrode.

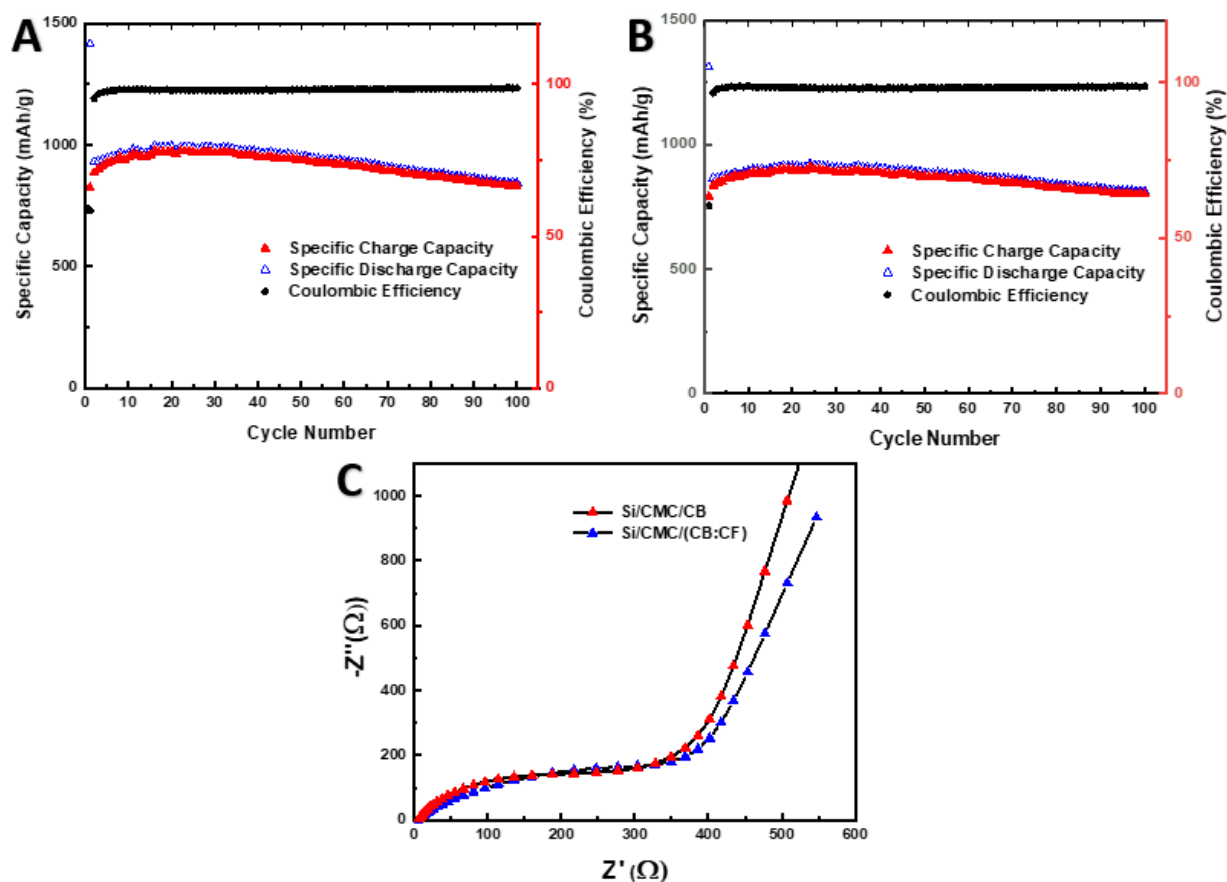


Figure 32. A. Cycle Performance of silicon slurry anodes. B. Cycle Performance of silicon/carbon fiber slurry anodes. C. Impedance plots of silicon and silicon/carbon fiber slurry anodes.

CHAPTER VI

CONCLUSION

Centrifugally spun carbon fibers from PAN precursors were used with a facile wet coating method to produce $\text{Co}_3\text{O}_4/\text{C}$ composite anodes for LIBs. The increase in active material concentration in the composite-fiber anode was achieved by using highly dispersed cobalt oxides/ethanol precursor solutions, and two-step heat treatment at a low carbonization temperature. The presence of the Co_3O_4 nanoparticles during heat treatment led to the incorporation of the nanoparticles into the carbon fibers through oxygen- and nitrogen-containing ligands in the carbonized PAN fibers. However, the presence of high concentration of nitrogen after carbonization indicated that the metal oxide nanoparticles were reduced to metallic cobalt and CoO by the nitrogen in the polymer. This method of fiber-composite processing allowed for the ease of production of coated polymer fibers. The difficulties associated with the centrifugal spinning of high viscosity solutions containing metallic (active material) nanoparticles were circumvented by using the proposed wet coating process, as desired high contents of active materials coated on PAN fibers were achieved. Coated carbon fibers yielded higher capacity with increased cobalt oxide concentration from 0 to 60 wt.%. The CCF composite anodes outperformed carbon fibers at a constant current density of 100 and 200 mA g^{-1} and showed a good capacity retention after 100 cycles.

Centrifugally spun Si/PVP fibers were successfully heat treated to form composite silicon/carbon fiber anodes. The electrochemical performance suggests CMC coatings on the silicon/carbon fiber composites can enhance the first cycle coulombic efficiency by increasing from 60% to 80%. When compared to silicon and silicon/carbon fiber slurry electrodes with CMC as binder, CMC coated silicon/carbon fiber composite performed better for the first ten cycles, as well as showing higher first cycle coulombic efficiencies. However, after 100 cycles, the silicon electrodes with the incorporation of carbon fibers outperformed the silicon fibers and the silicon electrode by itself. These results suggest that the addition of carbon fibers from centrifugally spun polymers can help alleviate the stress associated with volumetric change in charge/discharge cycles. Additionally, the coating method presented in this work can be used to address the problem of the large SEI formation in fibrous anodes. Furthermore, coating methods presented in this thesis can provide advantageous electrode production avenues which can unlock the potential of fibrous anode materials for LIBs.

CHAPTER VII

FUTURE WORK

Future work on this thesis would involve exploring the increased concentration of CMC in the silicon/carbon fiber composite anodes. From the experiments conducted, only two concentrations (10 and 20%) were explored. Significant improvements were done with the 20% CMC coatings; however, higher concentrations might further enhance the first cycle coulombic efficiency. However, to get good results for prolonged cycles, the amount of silicon must be lowered. Further studies into binder coatings and electrolyte additives could be explored and could be approached in a similar manner to the work presented in this thesis.

REFERENCES

1. Piccolino, M., *The bicentennial of the Voltaic battery (1800-2000): the artificial electric organ*. Trends Neurosci, 2000. **23**(4): p. 147-51.
2. Kragh, H., *Confusion and controversy: Nineteenth-century theories of the voltaic pile*. Kirjassa F. Bevilacqua ja EA Giannetto (Toim.) Nuova Voltiana, Studies on Volta and his Times, 2000. **1**: p. 133-157.
3. Besenhard, J.O., *Handbook of battery materials*. 2008: John Wiley & Sons.
4. Goodenough, J.B., *How we made the Li-ion rechargeable battery*. Nature Electronics, 2018. **1**(3): p. 204-204.
5. Roy, P. and S.K. Srivastava, *Nanostructured anode materials for lithium ion batteries*. Journal of Materials Chemistry A, 2015. **3**(6): p. 2454-2484.
6. Marom, R., et al., *A review of advanced and practical lithium battery materials*. Journal of Materials Chemistry, 2011. **21**(27): p. 9938-9954.
7. Reddy, M., G. Subba Rao, and B. Chowdari, *Metal oxides and oxysalts as anode materials for Li ion batteries*. Chemical reviews, 2013. **113**(7): p. 5364-5457.
8. Sun, H. and K. Zhao, *Electronic structure and comparative properties of $\text{LiNi}_x\text{Mn}_y\text{Co}_z\text{O}_2$ cathode materials*. The Journal of Physical Chemistry C, 2017. **121**(11): p. 6002-6010.
9. Lewandowski, A. and A. Świdorska-Mocek, *Ionic liquids as electrolytes for Li-ion batteries—an overview of electrochemical studies*. Journal of Power sources, 2009. **194**(2): p. 601-609.
10. Shin, J.-H., W.A. Henderson, and S. Passerini, *Ionic liquids to the rescue? Overcoming the ionic conductivity limitations of polymer electrolytes*. Electrochemistry Communications, 2003. **5**(12): p. 1016-1020.
11. Guerfi, A., et al., *Improved electrolytes for Li-ion batteries: Mixtures of ionic liquid and organic electrolyte with enhanced safety and electrochemical performance*. Journal of Power Sources, 2010. **195**(3): p. 845-852.

12. Yoshio, M., R.J. Brodd, and A. Kozawa, *Lithium-ion batteries*. Vol. 1. 2009: Springer
13. Goriparti, S., et al., *Review on recent progress of nanostructured anode materials for Li-ion batteries*. Journal of power sources, 2014. **257**: p. 421-443.
14. Zheng, Y., et al., *Lithium Distribution in Structured Graphite Anodes Investigated by Laser-Induced Breakdown Spectroscopy*. Applied Sciences, 2019. **9**(20): p. 4218.
15. Wagemaker, M. and F.M. Mulder, *Properties and promises of nanosized insertion materials for Li-ion batteries*. Accounts of chemical research, 2012. **46**(5): p. 1206-1215.
16. Martha, S.K., et al., *Li₄Ti₅O₁₂/LiMnPO₄ lithium-ion battery systems for load leveling application*. Journal of The Electrochemical Society, 2011. **158**(7): p. A790-A797.
17. Ponrouch, A. and M.R. Palacín, *Optimisation of performance through electrode formulation in conversion materials for lithium ion batteries: Co₃O₄ as a case example*. Journal of Power Sources, 2012. **212**: p. 233-246.
18. Poizot, P., et al., *Nano-sized transition-metal oxides as negative-electrode materials for lithium-ion batteries*. Nature, 2000. **407**(6803): p. 496.
19. Fang, S., D. Bresser, and S. Passerini, *Transition Metal Oxide Anodes for Electrochemical Energy Storage in Lithium-and Sodium-Ion Batteries*. Advanced Energy Materials, 2020. **10**(1): p. 1902485.
20. Bresser, D., S. Passerini, and B. Scrosati, *Leveraging valuable synergies by combining alloying and conversion for lithium-ion anodes*. Energy & Environmental Science, 2016. **9**(11): p. 3348-3367.
21. Liu, Z., et al., *Silicon oxides: a promising family of anode materials for lithium-ion batteries*. Chemical Society Reviews, 2019. **48**(1): p. 285-309.
22. Li, X., et al., *Germanium anode with excellent lithium storage performance in a germanium/lithium-cobalt oxide lithium-ion battery*. ACS nano, 2015. **9**(2): p. 1858-1867.
23. Wang, Y., et al., *Aluminum fumarate-based metal organic frameworks with tremella-like structure as ultrafast and stable anode for lithium-ion batteries*. Nano Energy, 2017. **39**: p. 200-210.
24. Jung, H., et al., *Amorphous silicon anode for lithium-ion rechargeable batteries*. Journal of power sources, 2003. **115**(2): p. 346-351.
25. Liu, W.-R., et al., *Enhanced cycle life of Si anode for Li-ion batteries by using modified elastomeric binder*. Electrochemical and Solid State Letters, 2004. **8**(2): p. A100.

26. Ding, N., et al., *Improvement of cyclability of Si as anode for Li-ion batteries*. Journal of Power Sources, 2009. **192**(2): p. 644-651.
27. Lestriez, B., et al., *On the binding mechanism of CMC in Si negative electrodes for Li-ion batteries*. Electrochemistry Communications, 2007. **9**(12): p. 2801-2806.
28. Obrovac, M. and L. Krause, *Reversible cycling of crystalline silicon powder*. Journal of The Electrochemical Society, 2007. **154**(2): p. A103-A108.
29. Bai, X., et al., *Si@ SiOx/graphene hydrogel composite anode for lithium-ion battery*. Journal of Power Sources, 2016. **306**: p. 42-48.
30. Hochgatterer, N.S., et al., *Silicon/graphite composite electrodes for high-capacity anodes: influence of binder chemistry on cycling stability*. Electrochemical and Solid State Letters, 2008. **11**(5): p. A76.
31. Xiong, Z., Y.S. Yun, and H.-J. Jin, *Applications of carbon nanotubes for lithium ion battery anodes*. Materials, 2013. **6**(3): p. 1138-1158.
32. Self, E.C., E.C. McRen, and P.N. Pintauro, *High Performance Particle/Polymer Nanofiber Anodes for Li-ion Batteries using Electrospinning*. ChemSusChem, 2016. **9**(2): p. 208-215.
33. Ji, L., et al., *Recent developments in nanostructured anode materials for rechargeable lithium-ion batteries*. Energy & Environmental Science, 2011. **4**(8): p. 2682-2699.
34. Yang, Z., J. Shen, and L.A. Archer, *An in situ method of creating metal oxide-carbon composites and their application as anode materials for lithium-ion batteries*. Journal of Materials Chemistry, 2011. **21**(30): p. 11092-11097.
35. Valdez, A., *Forcespinning of Metal Oxides and Metal Sulfides and Their Applications as Alternative Anode Materials for Lithium-ion and Sodium-ion Batteries*. 2018, The University of Texas Rio Grande Valley.
36. ZHANG, M., et al. *Electrospun Composite of Fe₃O₄/Cu Nanocrystals Encapsulated in Carbon Fibers as an Anode Material with High Rate Capability for Lithium Ion Batteries*. in *3rd International Conference on Material Engineering and Application (ICMEA 2016)*. 2016. Atlantis Press.
37. Dong, L., et al., *PVP-derived carbon nanofibers harvesting enhanced anode performance for lithium ion batteries*. RSC advances, 2016. **6**(5): p. 4193-4199.
38. Wang, P., et al., *Mesoporous carbon nanofibers with a high surface area electrospun from thermoplastic polyvinylpyrrolidone*. Nanoscale, 2012. **4**(22): p. 7199-7204.

39. Tang, K., et al., *Multichannel hollow TiO₂ nanofibers fabricated by single-nozzle electrospinning and their application for fast lithium storage*. *Electrochemistry Communications*, 2013. **28**: p. 54-57.
40. Campos, H., J. Ayala, and C. Valdes, *The use of Fe₃O₄/Carbon composite fibers as anode materials in lithium ion batteries*. *MOJ Poly Sci*, 2018. **2**(2): p. 44-46.
41. Valdez, A., et al., *MoS₂ and MoO₂ Loaded Carbon Microfibers as Anode Materials for Lithium-Ion and Sodium-Ion Batteries*. *ECS Transactions*, 2018. **85**(13): p. 357-368.
42. Mauger, A., H. Xie, and C.M. Julien, *Composite anodes for lithium-ion batteries: status and trends*. *AIMS Mater. Sci*, 2016. **3**(3): p. 1054-1106.
43. Chen, J., et al., *Unveiling the roles of binder in the mechanical integrity of electrodes for lithium-ion batteries*. *Journal of The Electrochemical Society*, 2013. **160**(9): p. A1502.
44. Komaba, S., et al., *Study on polymer binders for high-capacity SiO negative electrode of Li-ion batteries*. *The Journal of Physical Chemistry C*, 2011. **115**(27): p. 13487-13495.
45. Lee, C.H., et al., *Direct, operando observation of the bilayer solid electrolyte interphase structure: Electrolyte reduction on a non-intercalating electrode*. *Journal of power sources*, 2019. **412**: p. 725-735.
46. Key, B., et al., *Real-time NMR investigations of structural changes in silicon electrodes for lithium-ion batteries*. *Journal of the American Chemical Society*, 2009. **131**(26): p. 9239-9249.
47. Liu, L., et al., *Free-standing hollow carbon fibers as high-capacity containers for stable lithium metal anodes*. *Joule*, 2017. **1**(3): p. 563-575.
48. Fan, L.Z., et al., *Succinonitrile as a versatile additive for polymer electrolytes*. *Advanced Functional Materials*, 2007. **17**(15): p. 2800-2807.
49. Xu, K. and A. von Cresce, *Interfacing electrolytes with electrodes in Li ion batteries*. *Journal of Materials Chemistry*, 2011. **21**(27): p. 9849-9864.
50. Sarkar, K., et al., *Electrospinning to forcespinningTM*. *Materials today*, 2010. **13**(11): p. 12-14.
51. McEachin, Z. and K. Lozano, *Production and characterization of polycaprolactone nanofibers via forcespinningTM technology*. *Journal of Applied Polymer Science*, 2012. **126**(2): p. 473-479.
52. Jaumann, T., et al., *SEI-component formation on sub 5 nm sized silicon nanoparticles in Li-ion batteries: the role of electrode preparation, FEC addition and binders*. *Physical Chemistry Chemical Physics*, 2015. **17**(38): p. 24956-24967.

53. Liu, C., et al., *Tailor-made high-performance reverse osmosis membranes by surface fixation of hydrophilic macromolecules for wastewater treatment*. RSC advances, 2019. **9**(31): p. 17766-17777.
54. Nguyen, C.C., et al., *Systematic investigation of binders for silicon anodes: interactions of binder with silicon particles and electrolytes and effects of binders on solid electrolyte interphase formation*. ACS applied materials & interfaces, 2016. **8**(19): p. 12211-12220.
55. Do, J.-S. and C.-H. Weng, *Preparation and characterization of CoO used as anodic material of lithium battery*. Journal of power sources, 2005. **146**(1-2): p. 482-486.
56. Yao, W., J. Chen, and H. Cheng, *Platelike CoO/carbon nanofiber composite electrode with improved electrochemical performance for lithium ion batteries*. Journal of solid state electrochemistry, 2011. **15**(1): p. 183-188.
57. Zhang, L., et al., *Controllable synthesis of core-shell Co@ CoO nanocomposites with a superior performance as an anode material for lithium-ion batteries*. Journal of Materials Chemistry, 2011. **21**(45): p. 18279-18283.
58. Rai, A.K., et al., *One-step synthesis of CoO anode material for rechargeable lithium-ion batteries*. Ceramics International, 2013. **39**(8): p. 9325-9330.
59. Wang, G., et al., *Investigation of cobalt oxides as anode materials for Li-ion batteries*. Journal of Power Sources, 2002. **109**(1): p. 142-147.
60. Bredar, A.R., et al., *Electrochemical impedance spectroscopy of metal oxide electrodes for energy applications*. ACS Applied Energy Materials, 2020. **3**(1): p. 66-98.
61. Ma, T.Y., et al., *Metal-organic framework derived hybrid Co₃O₄-carbon porous nanowire arrays as reversible oxygen evolution electrodes*. Journal of the American Chemical Society, 2014. **136**(39): p. 13925-13931.
62. Manteghi, F., et al., *Preparation and application of cobalt oxide nanostructures as electrode materials for electrochemical supercapacitors*. RSC Advances, 2015. **5**(93): p. 76458-76463.
63. Li, M., et al., *Nanosilica/carbon composite spheres as anodes in Li-ion batteries with excellent cycle stability*. Journal of Materials Chemistry A, 2015. **3**(4): p. 1476-1482.
64. Ren, Y. and M. Li, *Si-SiO_x-cristobalite/graphite composite as anode for li-ion batteries*. Electrochimica Acta, 2014. **142**: p. 11-17.
65. Wang, C.-M., et al., *In situ TEM investigation of congruent phase transition and structural evolution of nanostructured silicon/carbon anode for lithium ion batteries*. Nano letters, 2012. **12**(3): p. 1624-1632.

APPENDIX

State-of-the-Art Equipment

Equipment	Purpose	Results Obtained
Scanning Electron Microscope	Measure fiber diameter and observe fiber characteristics	Measured the distribution of diameter in fibers to be in the order of a few microns.
TGA	To determine concentration of metal oxides or ceramic nanoparticles within the fibers	30, 50 and 60 percent of 10 mg samples were composed of Cobalt.
XPS	To see the oxidation state of Metal Oxide nanoparticles in the fibers	Distinguished CoO from Co ₃ O ₄ imbedded in the fiber matrix
Forcespinning Cyclone	Produce nano/microfibers	Mass produced fibers for applications in LIBs.
Metrohm Autolab Modular Potentiostat/Galvanostat	Measure Electrochemical Impedance of the cell	For Cobalt Oxide: cells were highly reactive to lithiation, no semicircle was found in the Real and Imaginary Impedance Spectra. For Silicon: Silicon Anodes show similar behavior to carbon anodes in terms of their diffusion and charge transfer resistance.
FiberRio FiberLab-L1000 Series	Generate carbon composite fibers	For use as Anode materials in lithium ion half-cell assemblies.

BioLogic	Perform Cyclic Voltametry Analysis of Lithium ion half-cells	Characterization of materials present in cobalt anodes based on their electrochemical activation potentials.
MBRAUN Glovebox	To use for assembling of cells, and preparation of electrolyte	

	under inert atmosphere and pressure	Produced more than 100 LIB half cells.
Lab View	Program and Analyze LANHE output	Evaluation of Cycle Performance in carbon composite fibers

Table 2. State-of-the-Art Software

Software	Purpose	Results Obtained
Nova 2.15	Simulations and analysis of results obtained from Metrohm Autolab Modular Potentiostat/Galvanostat	Correctly Modeled the charge transfer and diffusion of cells within an error margin of less than 5 % with the square means root method.
ARBIN	Create programs ie: Rate Performance, perform Galvanostatic analysis	Measured the Rate Performance of Lithium ion half-cell assemblies
BT Lab	Perform Cyclic Voltammetry Analysis of Lithium ion half-cells	Data to build report figures such Specific Current vs Voltage (CV)
LANHE	To implement galvanostatic charge discharge programs at fixed charge/discharge rates	Data to build report figures such as cycle performance and Charge/Discharge vs. Potentials curves
Origin	Creating figures for publication, from the instruments that provide data on cell performance.	Cell performance figures on Thesis including cycle /rate performance, impedance, and CV.

BIOGRAPHICAL SKETCH

Jonathan G. Ayala was born in San Nicolas de los Garza, Nuevo Leon, MX where he lived for the first seven years of his life and attended one semester of 1st grade at the elementary school at Escuela Primaria Frida Khalo. At the age of seven, Jonathan and his family moved to McAllen, TX. Here he learned English while attending Fields Elementary (1st through 5th), followed by Travis Middle School where he attended gifted and talented classes, and McAllen High school where he graduated in the top ten percentile. After graduating high school, Jonathan went on to The University of Texas Rio Grande, where he enrolled in the psychology program due to his interest in Neuroscience. Jonathan soon realized that a degree in psychology would not fulfill his satisfaction for finding a job that not only allowed him to support his family but provided a big challenge both academically and professionally. Soon after, Jonathan found Engineering, and saw that it provided the ability to solve some of the world's biggest problems, presented an academic challenge, and provided a great economic incentive. For this reason, Jonathan went on to finish the Engineering degree in 2019 with Magna Cum Laude honors and in May 2021, he was awarded Master of Science in Engineering in Mechanical Engineering from the University of Texas Rio Grande Valley. Always keen on keeping an open mind, his interest in the early development of electric vehicles led him to discover Dr. Alcoutlabi's lab where he worked in the field of rechargeable Lithium-ion batteries for two years as an undergraduate and throughout his master's education. After graduation, Jonathan hopes to continue to work in the field of electrochemistry. He can be contacted at jgayala51@gmail.com.